KINETIC AND RADIATIVE EXTINCTIONS OF SPHERICAL DIFFUSION FLAMES

A THESIS SUBMITTED TO THE GRADUATE DIVISION OF THE UNIVERSITY OF HAWAI'I IN PARTIAL FULFILLENT OF THE REQUIREMENTS FOR THE DEGREE OF

MASTER OF SCIENCE

IN

MECHANICAL ENGINEERING

AUGUST 2007

By
Qian Wang

Thesis Committee:

Beei-Huan Chao, Chairperson
Weilin Qu
Stephen M. Masutani

We certify that we have read this thesis and that, in our opinion, it is satisfactory in scope and quality as a thesis for the degree of Master of Science in Mechanical Engineering.

THESIS COMMITTEE

Chairperson

ACKNOWLEDGEMENTS

It would be impossible to lead to a master degree on Mechanical Engineering without incorporation the help and encouragement from people around me. Writing thesis won't be a fun thing to do if the previous research and study are not conducted carefully. Luckily, we did thorough and systematic preparation on equation derivation, program developing and numerical calculation, so the thesis writing was then reduced to a report of our effort, a record of study processes, I will say.

The first person to whom I would like to give my appreciation is Dr. Chao, Beei-Huan. It was him who provided the opportunity for me to study here and who gave me all the guidance constantly. Even before my first year classes officially started, he began to teach me and Karl the perturbation method every Wednesday in his office at POST building. I rapidly become ready for a serious scientific study because of these "private lectures". Sometimes, I forgot what he had explained to me for my questions right after I left his office. However, Dr. Chao, he is always very patient and took his time to repeat the important concepts over and over gain.

I would also like to thank my other two committee members-Dr. Qu, Weilin and Dr. Masutani, Stephen, for revising my draft and giving all the valuable suggestions. Thank both of them for encouraging and supporting me during my defense. Specially, Dr. Masutani is being very witty, for he has many challenging questions in mind and they will come out at any time. The defense was a pleasant time, during which I was inspired and knew my deficiency.

My thanks would not be completed without acknowledging the fund from NASA under contract #NCC3-1062 and the financial support from both Mechanical Engineering department, and Physics and Astronomy department for their teaching assistantship.

Finally and always, I would like to thank my parents for their love, tangible and intangible.

ABSTRACT

In this thesis, the effect of radiative heat loss on extinction of spherical diffusion flame stabilized by a spherical porous burner was investigated by activation energy asymptotics. The flow field was developed by issuing a reactant flow from the burner into a quiescent ambient filled with the other reactant. A one-step, overall and irreversible reaction that follows an Arrhenius kinetics with high activation energy was adopted to model the combustion reaction. The radiative heat loss rate was described by an optically thin model. Based on which reactant is supplied from the burner and how the inert gas is distributed, four model flames, namely the flames with fuel issuing into air, diluted fuel issuing into oxygen, air issuing into fuel, and oxygen issuing into diluted fuel were studied to understand the effects of stoichiometric mixture fraction and flow direction. Results show that when the flow rates fixed, only the conventional kinetic extinction limit at low Damköhler number (low residence times) was observed. The effect of radiative heat loss was to promote extinction such that it is easier to occur. By keeping the radiation intensity constant while varying the flow rate, both the kinetic and radiative extinction limits, representing the smallest and largest flow rates between which steady burning is possible, were exhibited. For flames with low radiation intensity, extinction was primarily characterized by the residence time such that the high-flow rate flames were easier to be quenched. As to the flames suffering strong radiative heat loss, extinction was dominated by the energy loss so the flame with larger size is weaker and easier to extinguish.

TABLE OF CONTENTS

LIST OF TABLES

LIST OF FIGURES

Figure Page

NOMENCLATURE

a	integration constant
B_K	pre-exponential factor of the combustion reaction
B_R	pre-exponential factor of the radiative heat loss
c_p	specific heat of the gas at constant pressure
D_i	mass diffusion coefficient of species i
Da_K	Damköhler number of the chemical reaction
Da_R	equivalent Damköhler number for the radiative heat loss
E_K	activation energy of the combustion reaction
E_R	equivalent activation energy of the radiative heat loss
F	fuel
m	mass flow rate
O	oxidizer
P	combustion products
q_1	heat of combustion per unit mass of the reactant supplied from the burner
R	Reactant
r	spatial coordinate in the radial direction
r_i	inner radius of the porous burner
r_b	outer radius of the porous burner
r_f	flame standoff location
T	temperature
T_0	supplied temperature of the gas at the center of the burner
T_b	temperature at the burner exit
T_f	flame temperature
T_i	temperature at the inner surface of the burner
T_∞	ambient temperature
u	radial flow velocity

W_i molecular weight of species i

Y_i mass fraction of species i

Greek Symbols

δ small expansion parameter defined as $\tilde{T}_f^2/\tilde{E}_R$

ε small expansion parameter defined as $\tilde{T}_f^2/\tilde{E}_K$

$\phi_{i,j}$ expansions of the reactant concentration functions in the reaction region

φ porosity (void space/total space) of the porous burner

κ Planck mean absorption coefficient

Λ_K reduced Damköhler number for the reaction

Λ_R equivalent reduced Damköhler number for the radiative heat loss

λ_g thermal conductivity of the gas

λ_s thermal conductivity of the solid material used to build the porous burner

$\tilde{\lambda}$ parameter defined as $\varphi + [(\lambda_s/\lambda_g)(1-\varphi)]$

ν_i stoichiometric coefficient of species i

Θ_j expansions of the temperature function in the radiation regions

θ_j expansions of the temperature function in the reaction region

ρ gas density

σ Stefan-Boltzmann constant

ξ stretched coordinate in the reaction region

ζ stretched coordinate in the radiation regions

Subscripts

0 specified value at the center of the burner

1 reactant supplied from the burner

2 ambient reactant

b	value of variables at the burner exit
f	value of variables at the flame sheet
i	quantities at the inner radius of the burner
P	combustion products
∞	specified value in the ambient

Superscripts

$\sim$	nondimensional quantities
-	solutions in the region between the burner exit and the flame sheet
+	solutions in the region outside of the flame sheet
–	rescaled variables

Chapter 1

Introduction

Prehistoric humans living in the glacial period had to struggle day and night against cold and hunger. By accident some of them discovered the use of fire, flame became a friend of human beings ever since. Caves that people resided in were lit and warmed up by smoldering branches of burning wood. Fire thus turned the cave into a cozy little room. They also found food tasted better when roasted, which completely changed our eating habit and food preparation processes. Fire which serves as an indispensable element in human life can sometimes lead to severe disasters if it is out of control. Taking a recent wildfire in Esperanza, Southern California on October 26, 2006 as an example, the fire burned an estimated 40,200 acres, resulting in the deaths of five firefighters, destroyed 34 houses and 20 outbuildings, and severely damaged California State Route 243 [1]. This incident demonstrated the cruel aspect of fire that it will become a major hazard to people's life and properties if not properly controlled. Concerning the safety and quality of human life, scientists and engineers have devoted tremendous effort to research activities on flame behaviors and control, such as ignition and flame suppression (extinction).

No less than the damage caused by unwanted fires, incomplete combustion and unsteady burning could also pose serious threats to people. These phenomena cause a weakening of burning and might result in undesired flame extinction. As a result, large quantities of pollutants are produced and precious fuels are wasted. A primary pollutant

that is produced through incomplete reaction is dark powdery soot. We see those powdery particles very often accumulated in chimneys and automobile mufflers, as well as emerging from the tail pipes of trucks and buses. It has been polluting our atmosphere and is hazardous to our lungs and general health when the particle is less than 5 micrometers in diameter, because it cannot be filtered out by our upper respiratory tract. On the positive side, soot can be utilized in many aspects. It has been used in early times as a source for carbon black, which is a common pigment used in paints and inks; and still is widely used in printing inks, toners for xerography, laser printers, and chemical industry nowadays [2]. From the stance of combustion, however, a steady, robust burning process is always desired to ensure better efficiency.

Extinction of diffusion flames has received tremendous attention in both theoretical and experimental combustion studies because of its fundamental and practical importance, though chemical and fluid mechanical complexities are always entwined. Examples of its application include loss of power in gas turbine engines and industrial furnaces, waste of fuels and pollution production from power plants, and issues related to fire safety. Theoretical analysis on extinction of diffusion flames was first performed by Fendell [3] in 1965. A detailed analysis of the structure and extinction of diffusion flames by means of a singular perturbation method was first reported in a seminal paper by Liñán in 1974 [4] through a one-dimensional counterflow diffusion flame. In his study, a one-step, overall and irreversible reaction that follows Arrhenius kinetics with high activation energy was considered. Heat loss from the flame was neglected such that the flame was assumed adiabatic. Flame extinction was observed at a minimum Damköhler number, below which steady burning is not possible. Damköhler number is

defined as the ratio of characteristic diffusion time to chemical reaction time. This extinction state exists because the reaction rate is too slow compared to the flow rate and the flame fails to sustain itself. It is observable without external energy loss and is later termed as the kinetic extinction limit. Excessive reactant leakage through flame and reduction in flame temperature from its adiabatic flame temperature are indications of extinction. The extinction state can therefore be identified by the use of Damköhler number.

The study was followed by Law [5] who analyzed the extinction of a flame surrounding a liquid fuel droplet and by Krishnamurthy et al. [6] who developed a similar asymptotic theory and successfully predicted the extinction limit of a stagnation-point flame established in a boundary layer. Later Chung and Law [7] generalized the study to other one-dimensional or quasi-one-dimensional diffusion flames and included the effect of Lewis number, which is defined as the ratio of the characteristic thermal diffusion rate to mass diffusion rate. The paper presented by Chung and Law showed that the structure equations for all one-dimensional or quasi-one-dimensional flames can be converted to the same form as that of Liñán by properly redefining parameters and therefore Liñán's results were readily applicable. Since then, extensive investigations on extinction of diffusion flames have been conducted theoretically, numerically and experimentally as reported in various journals [e.g. 8 – 13].

The influence of radiative heat transfer on the extinction of small diffusion flames at zero gravity environments was first reported by Bonne [14] who observed that without first depleting fuel and oxidant, radiative heat loss reduces flame temperature and thereby promotes extinction, while he did not mention whether the extinction occurs at a high

Damköhler number or if radiation promotes the kinetic extinction. However, because of the intrusion of buoyant force on Earth, which distorts the flame and reduces the residence time, radiative extinction is unlikely to occur on Earth and had not received much attention until the 1980s. In 1982, Sohrab et al. [15] analyzed a counterflow diffusion flame with radiation by using activation energy asymptotics. The extinction condition was obtained in terms of a Damköhler number. Although an analytical result was obtained by them, existence of a radiative extinction limit at high Damköhler numbers was not observed because the solution was not properly rescaled. Sibulkin [16] in his review paper discussed the effect of thermal radiation from the flame and the burning fuel surface on flame extinction. His numerical results showed how other factors (e.g. ambient oxygen concentration) affect extinction limits. However, the existence of radiative extinction was not explicitly mentioned. The possibility of having a radiative extinction limit at large Damköhler numbers other than the conventional kinetic extinction limit was first suggested by T'ien [17] from his numerical study of low stretch (long residence time) stagnation point flames with radiative heat loss from the surface of the condensed phase fuel (e.g., PMMA). His numerical results showed that there are an upper and a lower bound of Damköhler numbers beyond which no solution was found. Although he concluded that steady flames exist only for Damköhler numbers between those limits, it was not clear whether the upper limit was found due to numerical errors.

The existence of a radiative extinction limit at large Damköhler numbers was first unambiguously identified by Chao et al. [18] in 1990 from their analytical study on extinction of droplet combustion in a quiescent ambient using activation energy asymptotics. Their results clearly demonstrated the existence of dual extinction points,

the kinetic extinction limit at a minimum Damköhler number and the radiative extinction limit at a maximum Damköhler number. Quasi-steady burning is only possible for Damköhler numbers between these extremes. Since the Damköhler number is defined to be proportional to the droplet diameter for droplet burning, the study identifies a smallest droplet size below which the flame extinguishes as a result of low reaction rate (kinetic extinction), as is well known from early studies [e.g., 5], and a largest droplet size above which the flame also extinguishes because of the excessive radiative heat loss. The range of Damköhler number (droplet size) within which a flame exists reduces with higher heat loss intensity, and a flammability limit exists when the radiation intensity becomes too strong such that the two extinction limits coincide with each other. The upper extinction limit, which is also a result of low reaction rate where the kinetic limit is reached, while it is induced by the existence of radiation and a reduction of flame temperature, was called the radiative extinction limit by Chao et al.. To differentiate the two extinction limits, they introduced the terminology "kinetic extinction limit" to describe the conventional extinction limit at low Damköhler numbers. The radiative extinction limit does not exist without radiation. Although its existence was theoretically predicted, it is unlikely that the radiative extinction limit can be observed experimentally in droplet combustion because the droplet size will only decrease after ignition.

The work of Chao et al. [18] was followed by other researchers to further explore and verify the radiative extinction limit and the flammability limit. Chan [19] studied the effect of thermal radiation on extinction of methane-air flamelet for turbulent nonpremixed flame using a flame code that employed detailed chemistry and detailed transport properties. Their study successively predicted the flame behavior with good

quantitative agreement with experiments. Chao and Law [20] extended their work by analyzing the extinction caused by radiative loss from a hot solid fuel surface and the radiative extinction limit was again observed. Liu et al [21] analyzed the counterflow diffusion flames by large activation energy asymptotics and reconfirmed the existence of two extinction limits and inflammable limits. Maruta et al. [22] examined counterflow methane/air flames numerically and experimentally, and pointed out that the mechanism of extinction at low stretch rates (high Damköhler numbers) is the energy loss caused by radiative heat transfer. Mills and Matalon investigated the extinction of a spherical diffusion flame stabilized by a spherical porous burner with the radiation zone in the fuel side of and sufficiently away from the flame [23], and the radiative extinction limit was again observed. All these studies have proven that radiative heat loss induces a second flame extinction limit at large Damköhler numbers.

As mentioned earlier, it is unlikely that the radiative extinction limit exists in the normal-gravity flames because of the intrusion of buoyant force. It is possible, however, that the radiative extinction limit could be observed in microgravity because the mixing and preheating of reactants are accomplished by the single diffusive transport mechanism and long residence times are feasible. With the availability of microgravity facilities for experiments, including the 2.2s and 5.2s drop towers in the NASA Glenn Research Center, parabolic flights, Space Shuttle flights and International Space Station, attempts have been made to verify the existence of radiative extinction limit. The similarities and differences of the structure and stability of burner-stabilized flames in zero and normal gravity environments were studied and compared by Patnaik et al. [24]. Atreya and Agrawal [25] based on their numerical computations showed that flame radiation

substantially influences the extinction of diffusion flames in microgravity. The extinction of diffusion flames in microgravity is caused by longer residence time and the accumulation of combustion products in the flame zone which enhances gas radiation. Soot formation, if existed, further increases the intensity of radiative heat loss. A large number of microgravity experiments on methanol diffusion flames have been conducted by Zhang et al. [26] in both 4.5 s drop tower in MGLAB, Japan and 2.2 s drop tower in NASA Glenn Research Center through the combustion of liquid droplet for the simplicity in flame configuration. Experiments on radiative extinction have also been performed in Space Shuttle by Nayagam et al. [27] and Dietrich et al. [28] through the burning of a liquid droplet fuel and its existence was confirmed by these experiments. Experiments on combustion conducted in microgravity have shown that the flame characteristics in microgravity and that in normal gravities are significantly different from each other both qualitatively and quantitatively. Availability of research in microgravity is extremely crucial to strengthen our understanding of flame behavior, better use our limited fuel resources by combustion devices of improved designs, better control the combustion processes and minimize the loss and damage from unwanted fire incidences.

Although droplet combustion has the advantage of simplicity in geometry, the flame is inherently unsteady. Quasi-steady burning can be only achieved in ideal conditions. Moreover, since the flame continues to shrink after ignition, while radiative extinction only is observable by increasing the droplet size (flame size), whether the extinction limit that was observed in Refs. [27] and [28] is really a radiative extinction limit is questionable. An improvement can be made by adopting the burner-generated spherical diffusion flame with gaseous reactants. In this geometry, a truly steady state

flame can be achieved, and the flame size can be enlarged by raising the flow rate until extinction occurs so the radiative extinction limit can be clearly identified. In addition, the flow direction and flame structure, which are characterized by the stoichiometric mixture fraction, can be independently controlled. The stoichiometric mixture fraction is defined as

$$Z_{st} = Y_{O,b} / (Y_{O,b} + \sigma Y_{F,b}) \quad , \tag{1.1}$$

where

$$\sigma = (\nu_O W_O) / (\nu_F W_F) \quad , \tag{1.2}$$

which is the stoichiometric ratio of oxidizer to fuel mass, and the subscript "b" denotes conditions at the burner exit where reactants are supplied.

The flow direction is either from the fuel to the oxidizer by issuing the fuel into an oxidizing ambient, or from the oxidizer to the fuel by supplying the oxidizer at the burner and injecting it into a chamber filled with the fuel. The flame structure can be controlled by having part or all of the inert gas (e.g., nitrogen) extracted from the air and diverted to the fuel side. The redirection of the inert gas does not alter the adiabatic flame temperature because the stoichiometric relation remains unchanged. The benefit of using such flame configuration has been demonstrated in a numerical study by Tse et al. [29], and a numerical and experimental study by Santa et al. [30]. In the work by Santa et al., experiments were performed by using the 2.2 s drop facilities in the NASA Glenn Research Center, and the transient radiative extinction limit was obtained as a function of the flow rate, fuel type and flow direction. Related experiments were performed by Yoo et al. [31] in normal gravity.

Motivated by the flexibility in controlling the experiments and the ability to identify the radiative extinction limit of a spherical diffusion flame, and realizing that a theoretical investigation which can be used to predict the extinction and flammability limits has not been systemically performed, the primary objective of this paper is to extend the previous theoretical works by Chao et al. [18] and Mills and Matalon [23] to study the effects of residence time and flame structure on radiative extinction of diffusion flames stabilized by a porous burner. The analysis closely followed that of Chao et al. [18] with the problem definition and formulation properly modified to reflect the characteristics of burner-supported flames, which will be presented in Chapter 2. Activation energy asymptotics was adopted and the detailed analysis will be presented in Chapter 3. An optically thin radiation model was employed to simplify the analysis. The results and discussion will be reported in Chapters 4 and 5.

A primary reason for performing this investigation is to improve fire safety in space. Fire safety is a main concern of NASA in its fulfillment of the mission of space voyage such as Mars exploration [32]. Since external assistance is not available in spacecraft, any small fire can lead to a serious disaster and must be prevented. Microgravity combustion experiments performed by Freidman and Urban [33] revealed that flames and fires have completely different behaviors in space and on Earth so that the best methods to prevent, detect, and extinguish fires in a spacecraft are very different from those used on Earth. Table.1 lists some major differences in flame characteristics in space as compared to those on Earth. This means that fire protection systems used on Earth might not perform as expected in microgravity, and investigations on combustion in microgravity such as the present study is necessary. The results of this study and

related studies from the same group can be also applied to a better control of combustion processes and lead to improvements in fuel economy and reduction on pollutants production. The more we understand about fire, the better we can control it and save lives, property, and money.

Key Features of Fires in Low Gravity and Microgravity (Freidman & Urban, 2000)

Property	Trend	Remarks
Ignition	Promoted	- Thermally stressed components can overheat rapidly - Particulate spills form flammable aerosols that persist for long periods of time - Burning plastics eject hot material randomly and violently
Flame Appearance	Altered	- In quiescent environments, flames are often symmetrical in shape and nearly invisible - Under low rates of imposed air flow, flames intensify and become bright and sooty
Flammability and Flame-Spread Rate; Quiescent Conditions	Increased, in some cases to match or exceed normal-gravity levels	- Low-rate ventilating flows stimulate low-gravity fires and greatly extend their flammability range and flame-spread rates - Freely propagating flames tend to spread toward the "wind," or into the oxygen source
Detection Signatures	NA	- Flames are often cooler and less radiant - Average size and range of soot particle sizes are greater - Combustion product nature and quantities are altered

Table 1 Life Support and Habitation Navigation

Chapter 2

Formulation

The problem of interest in this study is a spherical diffusion flame burning at steady state and stabilized by a spherical porous burner, similar to that of Liu et al. [34], Mills and Matalon [23], Santa et al. [30], Sunderland et al. [35, 36], Tse et al. [29], and Yoo et al. [31], as shown schematically in Fig.2.1. The burner consists of a void core region at its center where the flow is supplied and a porous region in which the flow is regulated and made uniform at its exit.

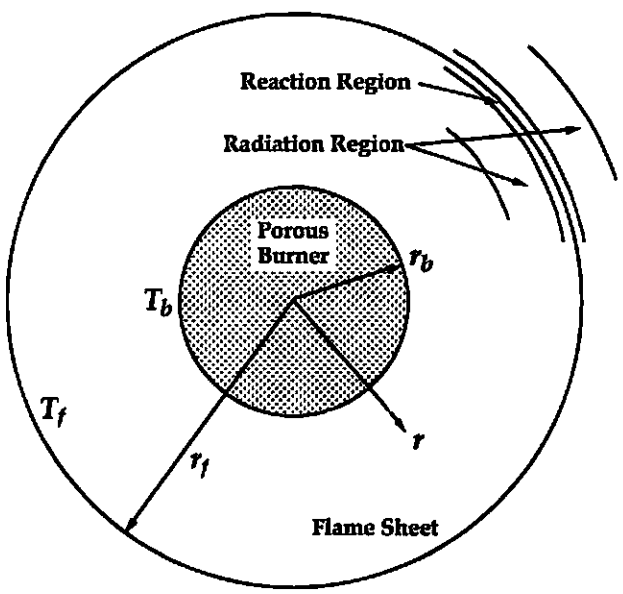

Figure 2.1 A schematic drawing of geometric configuration of the porous burner.

A reactant stream with a specified temperature of T_0 and mass fraction $Y_{1,0}$ is injected from the center of the burner into a quiescent environment filled with the other

reactant at a temperature of T_∞ and mass fraction of $Y_{2,\infty}$. The burner is assumed to be perfectly spherical and the effect of gravity is assumed negligible such that the flow is uniform in the radial direction, r, and the flame is spherical. The flow direction can be either from the fuel to the oxidizer by having the fuel issued from the burner and flows into the oxidizing environment (normal flame) or from the oxidizer to the fuel by having the oxidizer supplied from the burner and flows into the fuel environment (inverse flame). The flame structure (stoichiometric mixture fraction) can be varied by adjusting the amount of inert gas (nitrogen) that is supplied with the fuel or the oxidizer.

Conservation equations and boundary conditions

The combustion reaction is assumed to follow a one-step, overall and irreversible reaction between the fuel and oxidizer, given by

$$\nu_1 R_1 + \nu_2 R_2 \rightarrow \nu_P P \tag{2.1}$$

where ν is the stoichiometric coefficient and the subscripts "1" and "2" denote the reactants supplied from the burner and in the ambient, respectively. A second order Arrhenius kinetics with the reaction rate expressed by

$$B_K \rho^2 Y_1 Y_2 \exp(-E_K / T) \tag{2.2}$$

where T is the temperature, B_K is the pre-exponential factor, ρ the gas density, Y_i the mass fraction of species i, and E_K the activation temperature (activation energy divided by the universal gas constant) of the reaction. The activation temperature of the reaction is assumed to be much higher (high activation energy reaction) compared with the flame temperature, as is realistic for hydrocarbon/air flames. This means that the reaction rate is very sensitive to temperature variations such that the combustion reaction is only

significant in a thin region near which the maximum temperature is located.

The effect of radiative heat loss from the flame on flame extinction is the main focus of this thesis. The flame size is considered to be small compared to the absorption length of the radiation emitting gases such that the re-absorption of radiation energy by the gases is negligible and the radiation can be considered optically thin. Adopting the optically thin radiation model, the rate of heat loss per unit volume, $\dot{q}_R$, is given by $\dot{q}_R = 4\sigma k(T^4 - T_\infty^4)$ where $\sigma = 1.36\times10^{-8} cal/m^2-\text{sec}-K^4$ is the Stefan-Boltzmann constant and k is the Planck's mean absorption coefficient. Carbon dioxide and water vapor are considered to be the only gas species that contribute to the radiative loss so that $\kappa = x_{CO_2}\,\kappa_{CO_2} + x_{H_2O}\,\kappa_{H_2O}$ where x is the molar fraction. Because the radiative energy transferred to the burner and that is absorbed by it is negligibly small [35], the burner is assumed to be transparent in radiation. Because the radiative heat loss is also sensitive to temperature variations (proportional to T^4), $\dot{q}_R$ will be approximated by an Arrhenius type of rate function, $\dot{q}_R \approx B_R \exp(-E_R/T)$ where B_R is the equivalent pre-exponential factor and E_R the equivalent activation temperature. The value of E_R is much higher than the flame temperature but much smaller than E_K [18].

The flow is considered steady and isobaric. The solid and the gas are assumed to be in thermal equilibrium inside the burner such that temperature distribution of the gas and the solid are the same at the same radial distance from the center of the burner, that is vary only in the radial direction r. Following the above problem description, the mass conservation yields a constant mass flow rate, given by $m = 4\pi r^2 \rho u$ in the core region and the gas region outside of the burner, and $m = 4\pi r^2 \rho u \varphi$ in the porous region, where

m is the mass flow rate, u the radial flow velocity and φ is the porosity of the burner defined as the fraction of the void space. The equations governing the conservation of energy and species in different regions are

(a) Core region ($0 < r < r_i$)

$$Y_1 = Y_{1,0} \quad , \quad Y_2 = 0 \quad , \tag{2.3}$$

$$\rho u c_p \frac{dT}{dr} - \frac{1}{r^2}\frac{d}{dr}\left(\lambda_g r^2 \frac{dT}{dr}\right) = 0 \quad . \tag{2.4}$$

(b) Within the porous burner ($r_i < r < r_b$)

$$Y_1 = Y_{1,0} \quad , \quad Y_2 = 0 \quad , \tag{2.5}$$

$$\rho u c_p \varphi \frac{dT}{dr} - \frac{1}{r^2}\frac{\partial}{\partial r}\left\{[\lambda_g \varphi + \lambda_s(1-\varphi)] r^2 \frac{dT}{dr}\right\} = 0 \quad . \tag{2.6}$$

(C) Gas region external to the burner ($r_b < r < \infty$)

$$\rho u c_p \frac{dT}{dr} - \frac{1}{r^2}\frac{d}{dr}\left(\lambda_g r^2 \frac{dT}{dr}\right) = \nu_1 W_1 q_1 B \rho^2 Y_1 Y_2 \exp(-E_K/T) - 4\sigma\kappa(T^4 - T_\infty^4)$$

$$= \nu_1 W_1 q_1 B \rho^2 Y_1 Y_2 \exp(-E_K/T) - B_R \exp(-E_R/T) \quad , \tag{2.7}$$

$$\rho u \frac{dY_1}{dr} - \frac{1}{r^2}\frac{d}{dr}\left(\rho D_1 r^2 \frac{dY_1}{dr}\right) = -\nu_1 W_1 B \rho^2 Y_1 Y_2 \exp(-E_K/T) \quad , \tag{2.8}$$

$$\rho u \frac{dY_2}{dr} - \frac{1}{r^2}\frac{d}{dr}\left(\rho D_2 r^2 \frac{dY_2}{dr}\right) = -\nu_2 W_2 B \rho^2 Y_1 Y_2 \exp(-E_K/T) \quad . \tag{2.9}$$

In the above equations λ_g and λ_s are the thermal conductivity of the gas and the solid burner, respectively, c_p specific heat of the gas at constant pressure, and D_i the mass diffusion coefficient of species i. Equation (2.6) is obtained by combining the energy conservation equations for the gas and the solid burner after taking the thermal equilibrium assumption. Penetration of the ambient reactant into the burner is considered negligible so that the reactant concentration remains unchanged in the burner.

The boundary and interface conditions required to solve these equations are:

$$r=0: \quad T=T_0 \quad , \tag{2.10}$$

$$r=r_i: \quad T=T_i \quad , \tag{2.11a}$$

$$\lambda_g(dT/dr)_{r_i^-}=[\lambda_g\varphi+\lambda_s(1-\varphi)](dT/dr)_{r_i^+} \quad , \tag{2.11b}$$

$$r=r_b: \quad T=T_b \quad , \tag{2.12a}$$

$$[\lambda_g\varphi+\lambda_s(1-\varphi)](\partial T/\partial r)_{r_b^-}=\lambda_g(\partial T/\partial r)_{r_b^+} \quad , \tag{2.12b}$$

$$\rho u Y_1-(\rho D_1)(dY_1/dr)=\rho u Y_{1,0} \quad , \tag{2.12c}$$

$$\rho u Y_2-(\rho D_2)(dY_2/dr)=0 \quad , \tag{2.12d}$$

$$r\to\infty: \quad T\to T_\infty \quad , \quad Y_1\to 0 \quad , \quad Y_2\to Y_{2,\infty} \quad , \tag{2.13}$$

where r_i is the inner radius of the burner and r_b is the outer radius of the burner. The temperature at the inner and outer surfaces of the burner, T_i and T_b, will be determined from the analysis. Equations (2.11b) and (2.12b) mean that the heat flux transferred to the surface is balanced with the heat flux leaving the surface, while Eqs. (2.12c) and (2.12d) ensure that the flow rate of the reactants is conserved across the burner exit.

Nondimensionalization

Equations (2.3) – (2.13) can be nondimensionalized by introducing the following nondimensional quantities:

$$\tilde{T}=\frac{c_pT}{q_1Y_{1,0}} \quad , \quad \tilde{Y}_1=\frac{Y_1}{Y_{1,0}} \quad , \quad \tilde{Y}_2=\frac{\nu_1W_1Y_2}{\nu_2W_2Y_{1,0}} \quad , \quad \tilde{r}=\frac{r}{r_b} \quad , \quad \tilde{r}_i=\frac{r_i}{r_b} \quad ,$$

$$\tilde{E}_K=\frac{c_pE_K}{q_1Y_{1,0}} \quad , \quad \tilde{E}_R=\frac{c_pE_R}{q_1Y_{1,0}} \quad , \quad \tilde{m}=\frac{c_pm}{4\pi r_b\lambda_g} \quad , \quad \tilde{\lambda}=\varphi+(1-\varphi)\frac{\lambda_s}{\lambda_g} \quad ,$$

$$Da_K = \frac{B_K \nu_2 W_2 \rho^2 c_p r_b^2 Y_{1,0}}{\lambda_g} \quad , \quad Da_R = \frac{B_R c_p r_b^2}{q_1 Y_{1,0} \lambda_g} \quad .$$

The Lewis numbers of the reactants are assumed to be unity such that $\rho D_i = \lambda_g / c_p$.

Applying these nondimensional quantities to Eqs. (2.3 – 2.13), we obtain

(a) Core region ($0 < \tilde{r} < \tilde{r}_i$)

$$\tilde{Y}_1 = 1 \quad , \quad \tilde{Y}_2 = 0 \quad , \tag{2.14}$$

$$\frac{1}{\tilde{r}^2}\frac{\partial}{\partial \tilde{r}}\left(\tilde{m}\tilde{T} - \tilde{r}^2 \frac{\partial \tilde{T}}{\partial \tilde{r}}\right) = 0 \quad . \tag{2.15}$$

(b) Within the porous burner ($\tilde{r}_i < \tilde{r} < 1$)

$$\tilde{Y}_1 = 1 \quad , \quad \tilde{Y}_2 = 0 \quad , \tag{2.16}$$

$$\frac{1}{\tilde{r}^2}\frac{d}{d\tilde{r}}\left(\tilde{m}\tilde{T} - \tilde{\lambda}\tilde{r}^2 \frac{d\tilde{T}}{d\tilde{r}}\right) = 0 \quad . \tag{2.17}$$

(C) Gas region external to the burner ($1 < \tilde{r} < \infty$)

$$\frac{1}{\tilde{r}^2}\frac{d}{d\tilde{r}}\left(\tilde{m}\tilde{T} - \tilde{r}^2 \frac{d\tilde{T}}{d\tilde{r}}\right) = Da_K \tilde{Y}_1 \tilde{Y}_2 \exp(-\tilde{E}_K/\tilde{T}) - Da_R \exp(-\tilde{E}_R/\tilde{T}) \quad , \tag{2.18}$$

$$\frac{1}{\tilde{r}^2}\frac{d}{d\tilde{r}}\left(\tilde{m}\tilde{Y}_1 - \tilde{r}^2 \frac{d\tilde{Y}_1}{d\tilde{r}}\right) = -Da_K \tilde{Y}_1 \tilde{Y}_2 \exp(-\tilde{E}_K/\tilde{T}) \quad , \tag{2.19}$$

$$\frac{1}{\tilde{r}^2}\frac{d}{d\tilde{r}}\left(\tilde{m}\tilde{Y}_2 - \tilde{r}^2 \frac{d\tilde{Y}_2}{d\tilde{r}}\right) = -Da_K \tilde{Y}_1 \tilde{Y}_2 \exp(-\tilde{E}_K/\tilde{T}) \quad . \tag{2.20}$$

(D) Boundary and interface conditions

$$\tilde{r} = 0 \ : \quad \tilde{T} = \tilde{T}_0 \quad . \tag{2.21}$$

$$\tilde{r} = \tilde{r}_i \ : \quad \tilde{T} = \tilde{T}_i \quad , \tag{2.22a}$$

$$(d\tilde{T}/d\tilde{r})_{\tilde{r}_i^-} = \tilde{\lambda}(d\tilde{T}/d\tilde{r})_{\tilde{r}_i^+} \quad . \tag{2.22b}$$

$$\tilde{r}=1 \; : \quad \tilde{T}=\tilde{T}_b \quad , \tag{2.23a}$$

$$\tilde{\lambda}(d\tilde{T}/d\tilde{r})_{1^-}=(d\tilde{T}/d\tilde{r})_{1^+} \quad , \tag{2.23b}$$

$$\tilde{m}\tilde{Y}_1-(d\tilde{Y}_1/d\tilde{r})=\tilde{m} \quad , \tag{2.23c}$$

$$\tilde{m}\tilde{Y}_2-(d\tilde{Y}_2/d\tilde{r})=0 \quad . \tag{2.23d}$$

$$\tilde{r}\to\infty \; : \; \tilde{T}\to\tilde{T}_\infty \quad , \quad \tilde{Y}_1\to 0 \quad , \quad \tilde{Y}_2\to\tilde{Y}_{2,\infty} \quad . \tag{2.24}$$

Temperature distribution in the core region ($0<\tilde{r}<\tilde{r}_i$)

In the core region, multiplying Eq. (2.15) by $\tilde{r}^2$ and integrating the resulting equation once, yields

$$\tilde{m}\tilde{T}-\tilde{r}^2\frac{\partial\tilde{T}}{\partial\tilde{r}}=c \quad . \tag{2.25}$$

The integration constant c is determined by the application of Eq. (2.21) as $c=\tilde{m}\tilde{T}_0$. Integrating Eq. (2.25), with the determined c, subject to Eq. (2.22a) gives

$$\tilde{T}=\tilde{T}_0+(\tilde{T}_i-\tilde{T}_0)\exp[\tilde{m}(\tilde{r}_i^{-1}-\tilde{r}^{-1})] \quad . \tag{2.26}$$

Temperature distribution within the porous burner ($\tilde{r}_i<\tilde{r}<1$)

Similar to the core region, the solution of temperature field in the burner region can be obtained by integrating Eq. (2.17) twice subject to the interface conditions in Eqs. (2.22a) and (2.23a) as

$$\tilde{T}=\tilde{T}_i+(\tilde{T}_b-\tilde{T}_i)\frac{\exp[-\tilde{m}/(\tilde{\lambda}\tilde{r})]-\exp[-\tilde{m}/(\tilde{\lambda}\tilde{r}_i)]}{\exp(-\tilde{m}/\tilde{\lambda})-\exp[-\tilde{m}/(\tilde{\lambda}\tilde{r}_i)]} \quad . \tag{2.27}$$

Substituting Eqs. (2.26) and (2.27) into Eq. (2.22b), we determine the temperature at the inner surface of the burner, $\tilde{T}_i$, in terms of $\tilde{T}_b$ as

$$\tilde{T}_i = \tilde{T}_0 + (\tilde{T}_b - \tilde{T}_0)\exp[(\tilde{m}/\tilde{\lambda})(1-\tilde{r}_i^{-1})] \quad . \tag{2.28}$$

The conservation equations of energy and species in the gas region outside the burner, described by Eqs. (2.18) – (2.20) subject to the boundary and interface conditions in Eqs. (2.23) and (2.24), need to be solved by activation energy asymptotics. The procedures of solving these equations are presented in Chapter 3.

Chapter 3

Asymptotic Solution in the Gas Region

In the limit of large but finite activation energy, the chemical (combustion) reaction is very sensitive to temperature variations and only occurs in a thin reaction region near which the maximum temperature, defined as the flame sheet temperature, is attained. Away from this reaction region, the reaction is frozen because of the low gas temperature. As mentioned in Chapter 2, the radiative heat loss is also sensitive to temperature variations ($\sim T^4$) and can be approximated by an Arrhenius function. The heat loss is then significant only in a thin radiation region near the flame sheet similar to the combustion reaction. Because the equivalent activation energy of the radiative heat loss, E_R, is much lower than the activation energy of the combustion reaction, E_K, the radiation region in which radiation is significant is much broader than the reaction region. Based on this analysis, the whole gas region outside of the burner is divided into five sub-regions governed by different transport processes. There is a thin reaction region embedding the flame sheet, which is sandwiched by two broader but still thin radiation regions. These "reaction regions" are then surrounded by two broad, inert transport regions. The transport processes in the reaction region, radiation regions and transport regions are characterized by the balance between diffusion and reaction, diffusion and radiation, and diffusion and convection, respectively. Radiation is not important in the reaction region because it is a volumetric loss mechanism. It is negligible when the volume is narrow. Expressing the ratio of the characteristic length scale of the reaction

region to that of the transport region by ε and the ratio of the characteristic length scale of the radiation region to that of the transport region by δ, we have $\varepsilon << \delta << 1$ ($\tilde{E}_K >> \tilde{E}_R >> 1$). The small parameters ε and δ will be used in the asymptotic expansions.

Outer Solutions in the Gas Region

In the outer, transport regions away from the reaction and radiation zones, the conservation equations are governed by the balance between diffusion and convection processes. Both the reaction and radiation are frozen because of the low temperature such that Eqs. (2.18) – (2.20) are reduced to

$$\frac{d}{d\tilde{r}}\left(\tilde{m}\tilde{T}-\tilde{r}^2\frac{d\tilde{T}}{d\tilde{r}}\right)=\frac{d}{d\tilde{r}}\left(\tilde{m}\tilde{Y}_1-\tilde{r}^2\frac{d\tilde{Y}_1}{d\tilde{r}}\right)=\frac{d}{d\tilde{r}}\left(\tilde{m}\tilde{Y}_2-\tilde{r}^2\frac{d\tilde{Y}_2}{d\tilde{r}}\right)=0 \quad . \tag{3.1}$$

Designate the variables between the burner and the flame by superscript "–" and variables out side of the flame by "+", respectively. The boundary conditions in Eqs. (2.23) and (2.24) are modified to:

$$\tilde{r}=1 \ : \quad \tilde{T}^- = \tilde{T}_b \quad , \quad \tilde{\lambda}(d\tilde{T}_{burner}/d\tilde{r})_{1^-} = (d\tilde{T}^-/d\tilde{r})_{1^+} \quad , \tag{3.2a}$$

$$\tilde{m}\tilde{Y}_1^- - (d\tilde{Y}_1^-/d\tilde{r}) = \tilde{m} \quad , \quad \tilde{m}\tilde{Y}_2 - (d\tilde{Y}_2/d\tilde{r}) = 0 \quad ; \tag{3.2b}$$

$$\tilde{r}\to\infty \ : \ \tilde{T}^+ \to \tilde{T}_\infty \quad , \quad \tilde{Y}_1^+ \to 0 \quad , \quad \tilde{Y}_2^+ \to \tilde{Y}_{2,\infty} \quad . \tag{3.3}$$

Solving the three equations in Eq. (3.1) for both sides of the reaction/radiation regions subject to Eqs. (3.2) and (3.3) and then expanding the solutions in terms of the small expansion parameters δ and ε, we obtain the solutions

$$\tilde{T}^- = [\tilde{T}_0^- + \varepsilon\tilde{T}_1^- + O(\varepsilon^2)] + \delta[\tilde{T}_2^- + O(\varepsilon)] + O(\delta^2) \quad , \tag{3.4a}$$

$$\tilde{T}_0^- = \tilde{T}_0 + (\tilde{T}_{b,0} - \tilde{T}_0)\exp[\tilde{m}(1-\tilde{r}^{-1})] \quad , \tag{3.4b}$$

$$\tilde{T}_i^- = \tilde{T}_{b,i}\exp[\tilde{m}(1-\tilde{r}^{-1})] \quad , \quad i = 1, 2 \quad ; \tag{3.4c}$$

$$\tilde{T}^+ = [\tilde{T}_0^+ + \varepsilon\tilde{T}_1^+ + O(\varepsilon^2)] + \delta[\tilde{T}_2^+ + O(\varepsilon)] + O(\delta^2) \quad , \tag{3.5a}$$

$$\tilde{T}_0^+ = \tilde{T}_\infty + a_{T,0}^+[1-\exp(-\tilde{m}/\tilde{r})] \quad , \tag{3.5b}$$

$$\tilde{T}_i^+ = a_{T,i}^+[1-\exp(-\tilde{m}/\tilde{r})] \quad , \quad i = 1, 2 \quad ; \tag{3.5c}$$

$$\tilde{Y}_1^- = [\tilde{Y}_{1,0}^- + \varepsilon\tilde{Y}_{1,1}^- + O(\varepsilon^2)] + \delta[\tilde{Y}_{1,2}^- + O(\varepsilon)] + O(\delta^2) \quad , \tag{3.6a}$$

$$\tilde{Y}_{1,0}^- = 1 - a_{1,0}^-\exp(-\tilde{m}/\tilde{r}) \quad , \tag{3.6b}$$

$$\tilde{Y}_{1,i}^- = -a_{1,i}^-\exp(-\tilde{m}/\tilde{r}) \quad , \quad i = 1, 2 \quad ; \tag{3.6c}$$

$$\tilde{Y}_1^+ = [\tilde{Y}_{1,0}^+ + \varepsilon\tilde{Y}_{1,1}^+ + O(\varepsilon^2)] + \delta[\tilde{Y}_{1,2}^+ + O(\varepsilon)] + O(\delta^2) \quad , \tag{3.7a}$$

$$\tilde{Y}_{1,i}^+ = a_{1,i}^+[1-\exp(-\tilde{m}/\tilde{r})] \quad , \quad i = 0, 1, 2 \quad ; \tag{3.7b}$$

$$\tilde{Y}_2^- = [\tilde{Y}_{2,0}^- + \varepsilon\tilde{Y}_{2,1}^- + O(\varepsilon^2)] + \delta[\tilde{Y}_{2,2}^- + O(\varepsilon)] + O(\delta^2) \quad , \tag{3.8a}$$

$$\tilde{Y}_{2,i}^- = a_{2,i}^-\exp(-\tilde{m}/\tilde{r}) \quad , \quad i = 0, 1, 2 \quad ; \tag{3.8b}$$

$$\tilde{Y}_2^+ = [\tilde{Y}_{2,0}^+ + \varepsilon\tilde{Y}_{2,1}^+ + O(\varepsilon^2)] + \delta[\tilde{Y}_{2,2}^+ + O(\varepsilon)] + O(\delta^2) \quad , \tag{3.9b}$$

$$\tilde{Y}_{2,0}^+ = \tilde{Y}_{2,\infty} - a_{2,0}^+[1-\exp(-\tilde{m}/\tilde{r})] \quad , \tag{3.9b}$$

$$\tilde{Y}_{2,i}^+ = -a_{2,i}^+[1-\exp(-\tilde{m}/\tilde{r})] \quad , \quad i = 1, 2 \quad . \tag{3.9c}$$

In the above equations the a's are integration constants yet to be determined. Expanding the solutions and the temperature at the burner exit, $\tilde{T}_b$, in terms of δ and ε, are necessary because they are affected by both of the two singularities. The equations are not completely solved because there is only one boundary condition on each side of the

reaction regions.

Radiation active regions

In the $O(\delta)$ radiation regions, radiative heat loss is activated, which reduces the flame temperature. Combustion reaction still is negligible because of the low temperature such that the outer solutions of $\tilde{Y}_1^{\pm}$ and $\tilde{Y}_2^{\pm}$ are applicable. The energy conservation equation in these regions is then

$$\frac{1}{\tilde{r}^2}\frac{d}{d\tilde{r}}\left(\tilde{m}\tilde{T}-\tilde{r}^2\frac{d\tilde{T}}{d\tilde{r}}\right)=-Da_R\exp(-\tilde{E}_R/\tilde{T}) \quad . \tag{3.10}$$

To describe the flame behavior in these regions, a stretched coordinate, $\zeta=(\tilde{r}-\tilde{r}_f)/\delta$ where the small expansion parameter δ is defined as $\delta=\tilde{T}_f^2/\tilde{E}_R$, is defined. Moreover, because only an $O(\delta)$ temperature variation from the flame temperature, $\tilde{T}_f$, is allowed, the temperature profile is expanded as

$$\tilde{T}^{\pm}=[\tilde{T}_f-\varepsilon\Theta_2^{\pm}+O(\varepsilon^2)]-\delta[\Theta_1^{\pm}+\varepsilon\Theta_3^{\pm}+O(\varepsilon^2)]+O(\delta^2) \quad . \tag{3.11}$$

Applying the temperature expansion to the Arrhenius term in Eq. (3.10), we have

$$\begin{aligned}\exp(-\tilde{E}_R/\tilde{T})=\exp(-\tilde{E}_R/\tilde{T}_f)\exp(-\Theta_1^{\pm})\{[1-(\varepsilon/\delta)(\Theta_2^{\pm}+O(\varepsilon))\rangle \\ -\varepsilon\langle\Theta_3^{\pm}+(2\Theta_1^{\pm}\Theta_2^{\pm}/\tilde{T}_f)\rangle+\cdots]+O(\delta)\} \quad .\end{aligned} \tag{3.12}$$

Substituting Eqs. (3.11) and (3.12) into Eq. (3.10), expanding the resulting repression in terms of δ and ε, and then collecting those terms of the same order of magnitude, we obtain, for the three leading order terms,

$$d^2\Theta_1^{\pm}/d\zeta^2=-\Lambda_R\exp(-\Theta_1^{\pm}) \quad , \tag{3.13}$$

$$d^2\Theta_2^{\pm}/d\zeta^2 = \Lambda_R\,\Theta_2^{\pm}\exp(-\Theta_1^{\pm}) \quad , \tag{3.14}$$

$$\frac{d^2\Theta_3^{\pm}}{d\zeta^2} - \frac{\tilde{m}-2\tilde{r}_f}{\tilde{r}_f^{\,2}}\frac{d\Theta_2^{\pm}}{d\zeta} = \Lambda_R[\Theta_3^{\pm} + (2\Theta_1^{\pm}\Theta_2^{\pm}/\tilde{T}_f)]\exp(-\Theta_1^{\pm}) \quad , \tag{3.15}$$

where $\Lambda_R = \delta Da_R \exp(-\tilde{E}_R/\tilde{T}_f)$ is the equivalent reduced Damköhler number for radiative heat loss.

The required boundary conditions to solve Eqs. (3.13) – (3.15) can be obtained from matching the solutions of temperature in the outer regions with the solutions in the radiation regions as $\tilde{r} \to \tilde{r}_f$. Matching can be performed by first substituting the stretched variable, $\tilde{r} = \tilde{r}_f + \delta\zeta$, into Eqs. (3.4) and (3.5), expanding the resulting equation in terms of δ and ε, and collecting the terms of the same orders. Equating the resulting expressions with the solution in the radiation region in the limit of $\zeta \to \pm\infty$. Through the matching process, we first determine the solution of two constants, $\tilde{T}_{b,0}$ and $a_{T,0}^{+}$, in terms of $\tilde{T}_f$ as

$$\tilde{T}_{b,0} = \tilde{T}_0 + \{(\tilde{T}_f - \tilde{T}_0)/\exp[\tilde{m}(1-\tilde{r}_f^{\,-1})]\} \quad , \tag{3.16}$$

$$a_{T,0}^{+} = (\tilde{T}_f - \tilde{T}_\infty)/[1-\exp(-\tilde{m}/\tilde{r}_f)] \quad , \tag{3.17}$$

in which the leading order flame temperature $\tilde{T}_f$ still needs to be determined. In addition, the following matching conditions are obtained:

$$\Theta_1^{-}(\zeta \to -\infty) = -g_1^{-} - g_0^{-}\zeta \quad , \tag{3.18a}$$

$$\Theta_2^{-}(\zeta \to -\infty) = -\tilde{T}_{b,1}\exp[\tilde{m}(1-\tilde{r}_f^{\,-1})] \quad , \tag{3.18b}$$

$$(d\Theta_3^{-}/d\zeta)_{\zeta\to-\infty} = -\tilde{T}_{b,1}(\tilde{m}/\tilde{r}_f^{\,2})\exp[\tilde{m}(1-\tilde{r}_f^{\,-1})] \quad , \tag{3.18c}$$

$$\Theta_1^+(\zeta \to \infty) = -g_1^+ + g_0^+ \zeta \quad , \tag{3.19a}$$

$$\Theta_2^+(\zeta \to \infty) = -a_{T,1}^+[1-\exp(-\tilde{m}/\tilde{r}_f)] \quad , \tag{3.19b}$$

$$(d\Theta_3^+/d\zeta)_{\zeta\to\infty} = a_{T,1}^+(\tilde{m}/\tilde{r}_f{}^2)\exp(-\tilde{m}/\tilde{r}_f) \quad , \tag{3.19c}$$

where

$$g_0^- = (\tilde{T}_f - \tilde{T}_0)(\tilde{m}/\tilde{r}_f{}^2) \quad , \tag{3.20a}$$

$$g_1^- = \tilde{T}_{b,2}\exp[\tilde{m}(1-\tilde{r}_f{}^{-1})] \quad , \tag{3.20b}$$

$$g_0^+ = (\tilde{T}_f - \tilde{T}_\infty)(\tilde{m}/\tilde{r}_f{}^2)/[\exp(-\tilde{m}/\tilde{r}_f)-1] \quad , \tag{3.21a}$$

$$g_1^+ = a_{T,2}^+[1-\exp(-\tilde{m}/\tilde{r}_f)] \quad . \tag{3.21b}$$

The parameters g_0^- and g_0^+ are defined such that they are positive constants.

The solutions of temperature can be determined by solving Eqs. (3.13) – (3.15) subject to the matching conditions in Eqs (3.18) – (3.21). Equation (3.13) can be solved by first multiplying the equation by $d\Theta_1^\pm$, and rearranging to obtain

$$d(d\Theta_1^\pm/d\zeta)^2 = 2\Lambda_R\, d[\exp(-\Theta_1^\pm)] \quad , \tag{3.22a}$$

and then integrating it once subject to Eqs. (3.18a) and (3.18b) to

$$(d\Theta_1^\pm/d\zeta)^2 = 2\Lambda_R\exp(-\Theta_1^\pm) + (g_0^\pm)^2 \quad . \tag{3.22b}$$

Integrating Eq. (3.22b) one more time subject to Eqs. (3.18a) and (3.19a) then yields

$$\Theta_1^\pm = \ell n\{1-[\Lambda_R/\langle 2(g_0^\pm)^2\rangle]\exp(g_1^\pm \mp g_0^\pm\zeta)\}^2 \pm g_0^\pm\zeta - g_1^\pm \quad , \tag{3.23}$$

which can be differentiated to

$$\frac{d\Theta_1^\pm}{d\zeta} = \pm g_0^\pm \frac{1+\{\Lambda_R/[2(g_0^\pm)^2]\}\exp(g_1^\pm \mp g_0^\pm\zeta)}{1-\{\Lambda_R/[2(g_0^\pm)^2]\exp(g_1^\pm \mp g_0^\pm\zeta)} \quad , \tag{3.24}$$

Next, Eq. (3.14) is integrated subject to Eqs. (3.18b) and (3.19b) by a similar approach,

but the procedure is more involved, giving the solution

$$\Theta_2^- = (\tilde{T}_{b,1}/g_0^-)\exp[\tilde{m}(1-\tilde{r}_f^{-1})](d\Theta_1^-/d\zeta) \quad , \tag{3.25}$$

$$\Theta_2^+ = -(a_{T,1}^+/g_0^+)[1-\exp(-\tilde{m}/\tilde{r}_f)](d\Theta_1^+/d\zeta) \quad . \tag{3.26}$$

Equation (3.15) is the most perplexing one among the three equations and the analysis is the most complicated. After a lengthy mathematical exercise and with the application of Eqs. (3.18c), (3.19c) and (3.23) – (3.26), we obtain

$$\begin{aligned}
\Theta_3^\pm = \mp & \left[\frac{8}{3}g_2^\pm g_0^\pm - \frac{1}{g_0^\pm}\left(\frac{d\tilde{T}_1^\pm}{d\tilde{r}}\right)_{\tilde{r}_f}\right]\left\{2+\frac{\sqrt{2\Lambda_R\exp(-\Theta_1^\pm)+(g_0^\pm)^2}}{g_0^\pm}\cdot\right. \\
& \left.\left\langle \ell n\left[\frac{2(g_0^\pm)^2}{\Lambda_R}\frac{\sqrt{2\Lambda_R\exp(-\Theta_1^\pm)+(g_0^\pm)^2}-g_0^\pm}{\sqrt{2\Lambda_R\exp(-\Theta_{,1}^\pm)+(g_0^\pm)^2}+g_0^\pm}\right]-2\right\rangle\right\} \\
& \pm\frac{g_2^\pm}{2}\sqrt{2\Lambda_R\exp(-\Theta_1^\pm)+(g_0^\pm)^2}\cdot \\
& \left\{\left\langle \ell n\left[\frac{2(g_0^\pm)^2}{\Lambda_R}\frac{\sqrt{2\Lambda_R\exp(-\Theta_1^\pm)+(g_0^\pm)^2}-g_0^\pm}{\sqrt{2\Lambda_R\exp(-\Theta_1^\pm)+(g_0^\pm)^2}+g_0^\pm}\right]\right\rangle^2-(\Theta_1^\pm)^2\right\} \\
& \pm 2g_2^\pm g_0^\pm\left\{\ell n\left[\frac{2(g_0^\pm)^2}{\Lambda_R}\frac{\sqrt{2\Lambda_R\exp(-\Theta_1^\pm)+(g_0^\pm)^2}-g_0^\pm}{\sqrt{2\Lambda_R\exp(-\Theta_1^\pm)+(g_0^\pm)^2}+g_0^\pm}\right]\right\} \\
& -\frac{\tilde{T}_3^\pm(\tilde{r}_f)+h_1^\pm}{g_0^\pm}\sqrt{2\Lambda_R\exp(-\Theta_1^\pm)+(g_0^\pm)^2}+h_1^\pm \\
& \mp\frac{g_1^\pm}{g_0^\pm}\left(\frac{d\tilde{T}_1^\pm}{d\tilde{r}}\right)_{\tilde{r}_f}\frac{\sqrt{2\Lambda_R\exp(-\Theta_1^\pm)+(g_0^\pm)^2}}{g_0^\pm} \\
& \mp\frac{2}{3}g_2^\pm\Theta_1^\pm\sqrt{2\Lambda_R\exp(-\Theta_1^\pm)+(g_0^\pm)^2} \quad ,
\end{aligned} \tag{3.27}$$

where

$$g_2^- = [2/(3\tilde{T}_f)](\tilde{T}_{b,1}/g_0^-)\exp[\tilde{m}(1-\tilde{r}_f^{-1})] \quad , \tag{3.28a}$$

$$g_2^+ = -[2/(3\tilde{T}_f)](a_{T,1}^+/g_0^+)[1-\exp(-\tilde{m}/\tilde{r}_f)] \quad , \tag{3.28b}$$

$$h_1^- = [(\tilde{m}-2\tilde{r}_f)/\tilde{r}_f^{\,2}](\tilde{T}_{b,1}/g_0^-)\exp[\tilde{m}(1-\tilde{r}_f^{-1})] \quad , \tag{3.28c}$$

$$h_1^+ = -[(\tilde{m}-2\tilde{r}_f)/\tilde{r}_f^{\,2}](a_{T,1}^+/g_0^+)[1-\exp(-\tilde{m}/\tilde{r}_f)] \quad . \tag{3.28d}$$

As will be shown later, $(d\Theta_3^{\pm}/d\zeta)$ is only needed in this work. Differentiating Eq. (3.27) with respect to ζ results in

$$\frac{d\Theta_3^{\pm}}{d\zeta}=\left[\frac{8}{3}g_2^{\pm}-\frac{1}{(g_0^{\pm})^2}\left(\frac{d\tilde{T}_1^{\pm}}{d\tilde{r}}\right)_{\tilde{r}_f}\right]\Big\{g_0^{\pm}\sqrt{2\Lambda_R\exp(-\Theta_1^{\pm})+(g_0^{\pm})^2}$$

$$+\Lambda_R\exp(-\Theta_1^{\pm})\left\langle \ell n\left[\frac{2(g_0^{\pm})^2}{\Lambda_R}\frac{\sqrt{2\Lambda_R\exp(-\Theta_1^{\pm})+(g_0^{\pm})^2}-g_0^{\pm}}{\sqrt{2\Lambda_R\exp(-\Theta_1^{\pm})+(g_0^{\pm})^2}+g_0^{\pm}}\right]-2\right\rangle\Big\}$$

$$-\frac{g_2^{\pm}}{2}\Lambda_R\exp(-\Theta_1^{\pm})\left\{\left\langle \ell n\left[\frac{2(g_0^{\pm})^2}{\Lambda_R}\frac{\sqrt{2\Lambda_R\exp(-\Theta_1^{\pm})+(g_0^{\pm})^2}-g_0^{\pm}}{\sqrt{2\Lambda_R\exp(-\Theta_1^{\pm})+(g_0^{\pm})^2}+g_0^{\pm}}\right]\right\rangle^2-(\Theta_1^{\pm})^2\right\}$$

$$-g_2^{\pm}g_0^{\pm}\sqrt{2\Lambda_R\exp(-\Theta_1^{\pm})+(g_0^{\pm})^2}\,\ell n\left[\frac{2(g_0^{\pm})^2}{\Lambda_R}\frac{\sqrt{2\Lambda_R\exp(-\Theta_1^{\pm})+(g_0^{\pm})^2}-g_0^{\pm}}{\sqrt{2\Lambda_R\exp(-\Theta_1^{\pm})+(g_0^{\pm})^2}+g_0^{\pm}}\right]$$

$$-g_2^{\pm}[2\Lambda_R\exp(-\Theta_1^{\pm})+(g_0^{\pm})^2]\left(\Theta_1^{\pm}+\frac{2}{3}\right)-2g_2^{\pm}(g_0^{\pm})^2$$

$$+\left[\pm\frac{\tilde{T}_3^{\pm}(\tilde{r}_f)+h_1^{\pm}}{g_0^{\pm}}+\frac{g_1^{\pm}}{(g_0^{\pm})^2}\left(\frac{d\tilde{T}_1^{\pm}}{d\tilde{r}}\right)_{\tilde{r}_f}+\frac{2}{3}g_2^{\pm}\Theta_1^{\pm}\right]\Lambda_R\exp(-\Theta_1^{\pm}) \quad . \qquad (3.29)$$

Subtracting the expression of $(d\Theta_3^{-}/d\zeta)$ at $\zeta = 0$ from that of $(d\Theta_3^{+}/d\zeta)$, and recognizing that the result should hold true in the non-radiative limit, we find

$$(d\Theta_3^{+}/d\zeta)_{\zeta=0}-(d\Theta_3^{-}/d\zeta)_{\zeta=0}$$

$$=(a_{T,1}^{+}/g_0^{+})(\tilde{m}/\tilde{r}_f{}^2)\exp(-\tilde{m}/\tilde{r}_f)[(g_0^{+})^2+2\Lambda_R]^{1/2}$$

$$+(\tilde{T}_{b,1}/g_0^{-})(\tilde{m}/\tilde{r}_f{}^2)\exp[\tilde{m}(1-\tilde{r}_f{}^{-1})][(g_0^{-})^2+2\Lambda_R]^{1/2} \quad . \qquad (3.30)$$

Inner expansion

In the $O(\varepsilon)$ inner reaction zone, only an $O(\varepsilon)$ variation of variables and an $O(\varepsilon)$ leakage of reactants are allowed. As a result, the temperature is within an $O(\varepsilon)$

reduction from the maximum temperature $\tilde{T}_f$ and the reactant mass fractions are $O(\varepsilon)$ quantities. Similar to the analysis in the radiation region, the stretched spatial coordinate in this region is defined as $\xi = (\tilde{r} - \tilde{r}_f)/\varepsilon$ where $\varepsilon = \tilde{T}_f^{\,2} / \tilde{E}_K$, and the temperature, fuel and oxidizer mass fraction distributions are expanded as

$$\tilde{T} = [\tilde{T}_f - \varepsilon\theta_1 - \varepsilon^2\theta_2 + O(\varepsilon^3)] + O(\delta) + O(\varepsilon/\delta) \quad , \tag{3.31}$$

$$\tilde{Y}_1 = [\varepsilon\phi_{1,1} + \varepsilon^2\phi_{1,2} + O(\varepsilon^3)] + O(\delta) + O(\varepsilon/\delta) \quad , \tag{3.32}$$

$$\tilde{Y}_2 = [\varepsilon\phi_{2,1} + \varepsilon^2\phi_{2,2} + O(\varepsilon^3)] + O(\delta) + O(\varepsilon/\delta) \quad . \tag{3.33}$$

As in Eq. (3.12), the controlling Arrhenius term in the reaction region is expanded as

$$\exp(-\tilde{E}_K/\tilde{T}) = \exp(-\tilde{E}_K/\tilde{T}_f)\exp(-\theta_1) + \ldots \quad . \tag{3.34}$$

Substituting the stretched coordinate, ξ, as well as Eqs. (3.31) and (3.34) into Eq. (2.18), expanding and collecting the leading orders of ε, we obtain a structure equation in this region,

$$d^2\theta_1/d\xi^2 = \Lambda_K\,\phi_{1,1}\,\phi_{2,1}\exp(-\theta_1) \quad , \tag{3.35}$$

where $\Lambda_K = \varepsilon^3 Da_K \exp(-\tilde{E}_K/\tilde{T}_f)$ is the reduced Damköhler number for the combustion reaction. As mentioned before, the radiation term is a higher order term in this region and the effect of radiative heat loss is secondary because the volume of the reaction region is much smaller than that of the radiation regions.

Next, subtracting Eq. (2.20) from Eq. (2.19) to eliminate the reaction term, then substituting Eqs. (3.32), (3.33) and ξ into the resulting equation, expanding in orders of ε and δ, and keeping terms of the two leading orders in ε, or $O(\varepsilon)$ and $O(\varepsilon^2)$ we have the specie-specie coupling functions

$$\phi_{1,1} - \phi_{2,1} = c_1 \xi + c_2 \quad , \tag{3.36}$$

$$\frac{d(\phi_{1,2} - \phi_{2,2})}{d\xi} + \frac{2}{\tilde{r}_f} \frac{d(\phi_{1,1} - \phi_{2,1})}{d\xi} \xi - \frac{\tilde{m}}{\tilde{r}_f^{\,2}} (\phi_{1,1} - \phi_{2,1}) = c_3 \quad , \tag{3.37}$$

where the c's are integration constants that need to be determined. Equation (3.36) is the result after the original differential equation is integrated twice and Eq. (3.37) is the result after the original equation is integrated once.

Finally, subtracting Eq. (2.19) from Eq. (2.18) and doing the expansion similar to the procedure used in obtaining Eqs. (3.36) and (3.37), we have the temperature-specie coupling functions,

$$\theta_1 - \phi_{1,1} = c_4 \xi + c_5 \quad , \tag{3.38}$$

$$\frac{d(\theta_2 - \phi_{1,2})}{d\xi} + \frac{2}{\tilde{r}_f} \frac{d(\theta_1 - \phi_{1,1})}{d\xi} \xi - \frac{\tilde{m}}{\tilde{r}_f^{\,2}} (\theta_1 - \phi_{1,1}) = c_6 \quad . \tag{3.39}$$

As the analysis performed in the radiation regions, the boundary conditions required to solve Eqs. (3.35) – (3.39) are derived from matching the inner solutions when $\xi \to \pm\infty$ with the outer solutions of $\tilde{Y}_1$ and $\tilde{Y}_2$ as $\tilde{r} \to \tilde{r}_f$, and the solutions of $\tilde{T}$ in the radiation regions as $\zeta \to 0$. For the species equations, matching is performed by substituting the stretched coordinate, $\tilde{r} = \tilde{r}_f + \varepsilon\xi$, into Eqs. (3.6) – (3.9), expanding and rearranging in orders of ε and δ, and equating the resulting expressions with Eqs. (3.32) and (3.33) to yield the solutions of some integration constants

$$a_{1,0}^{-} = \exp(\tilde{m}/\tilde{r}_f) \quad , \quad a_{1,0}^{+} = a_{1,2}^{-} = a_{1,2}^{+} = 0 \quad , \tag{3.40}$$

$$a_{2,0}^{+} = \tilde{Y}_{2,\infty}/[1 - \exp(-\tilde{m}/\tilde{r}_f)] \quad , \quad a_{2,0}^{-} = a_{2,2}^{-} = a_{2,2}^{+} = 0 \quad , \tag{3.41}$$

and the matching conditions

$$\phi_{1,1}(\xi \to -\infty) = -a_{1,1}^{-} \exp(-\tilde{m}/\tilde{r}_f) - (\tilde{m}/\tilde{r}_f{}^2)\xi \quad , \tag{3.42}$$

$$\phi_{1,1}(\xi \to \infty) = a_{1,1}^{+}[1 - \exp(-\tilde{m}/\tilde{r}_f)] \quad , \tag{3.43}$$

$$[(d\phi_{1,2}/d\xi) + (2/\tilde{r}_f)(d\phi_{1,1}/d\xi)\xi - (\tilde{m}/\tilde{r}_f{}^2)\phi_{1,1}]_{\xi \to -\infty} = 0 \quad , \tag{3.44}$$

$$[(d\phi_{1,2}/d\xi) + (2/\tilde{r}_f)(d\phi_{1,1}/d\xi)\xi - (\tilde{m}/\tilde{r}_f{}^2)\phi_{1,1}]_{\xi \to \infty} = -a_{1,1}^{+}(\tilde{m}/\tilde{r}_f{}^2) \quad , \tag{3.45}$$

$$\phi_{2,1}(\xi \to -\infty) = a_{1,1}^{-} \exp(-\tilde{m}/\tilde{r}_f) \quad , \tag{3.46}$$

$$\phi_{2,1}(\xi \to \infty) = -a_{2,1}^{+}[1 - \exp(-\tilde{m}/\tilde{r}_f)] + \{\tilde{Y}_{2,\infty}(\tilde{m}/\tilde{r}_f{}^2)/[\exp(\tilde{m}/\tilde{r}_f) - 1]\}\xi \quad , \tag{3.47}$$

$$[(d\phi_{2,2}/d\xi) + (2/\tilde{r}_f)(d\phi_{2,1}/d\xi)\xi - (\tilde{m}/\tilde{r}_f{}^2)\phi_{2,1}]_{\xi \to -\infty} = 0 \quad , \tag{3.48}$$

$$[(d\phi_{2,2}/d\xi) + (2/\tilde{r}_f)(d\phi_{2,1}/d\xi)\xi - (\tilde{m}/\tilde{r}_f{}^2)\phi_{2,1}]_{\xi \to \infty} = a_{2,1}^{+}(\tilde{m}/\tilde{r}_f{}^2) \quad . \tag{3.49}$$

For the energy equation, the solutions in the inner region and those of the radiation regions are matched in their common regions. Realizing that $\tilde{r} = \tilde{r}_{f,s} + \delta\zeta = \tilde{r}_{f,s} + \varepsilon\xi$, matching is performed by expressing Eq. (3.11) in terms of $\zeta = (\varepsilon/\delta)\xi$, expanding and rearranging in orders of ε and δ, and equating the resulting expressions with Eqs. (3.31). The results of matching, including the solutions of some constants and the matching conditions, are listed in the following:

$$g_1^{\pm} = -2\ln\{[\langle 1 + [2\Lambda_R/(g_0^{\pm})^2]\rangle^{1/2} + 1]/2\} \quad , \tag{3.50}$$

$$\tilde{T}_{b,2} = -2\ln\{[\langle 1 + [2\Lambda_R/(g_0^{-})^2]\rangle^{1/2} + 1]/2\}\exp[\tilde{m}(\tilde{r}_f{}^{-1} - 1)] \quad , \tag{3.51}$$

$$a_{T,2}^{+} = -2\ln\{[\langle 1 + [2\Lambda_R/(g_0^{+})^2]\rangle^{1/2} + 1]/2\}/[1 - \exp(-\tilde{m}/\tilde{r}_f)] \quad , \tag{3.52}$$

$$\theta_1(\xi \to -\infty) = -\{(\tilde{T}_{b,1}/g_0^-)\exp[\tilde{m}(1-\tilde{r}_f^{-1})] + \xi\}[(g_0^-)^2 + 2\Lambda_R]^{1/2} \quad , \quad (3.53)$$

$$\theta_1(\xi \to \infty) = -\{(a_{T,1}^+/g_0^+)[1-\exp(-\tilde{m}/\tilde{r}_f)] - \xi\}[(g_0^+)^2 + 2\Lambda_R]^{1/2} \quad , \quad (3.54)$$

$$(d\theta_2/d\xi)_{\xi \to \pm\infty} = (d\Theta_3^{\pm}/d\zeta)_{\zeta=0} + (d^2\Theta_4^{\pm}/d\zeta^2)_{\zeta=0}\xi \quad . \quad (3.55)$$

Inner solutions

The inner equations are solved by first substituting Eqs. (3.44) and (3.48) into Eq. (3.37) to find $c_3 = 0$, then substituting Eqs. (3.45) and (3.49) into the resulting equation and yields

$$a_{1,1}^+ + a_{2,1}^+ = 0 \quad \text{or} \quad a_{2,1}^+ = -a_{1,1}^+ \quad . \quad (3.56)$$

It is followed by substituting Eqs. (3.42) and (3.46) into Eq. (3.36). to determine c_1 and c_2, then substituting Eqs. (3.43) and (3.47) into the resulting equation, which gives

$$\tilde{r}_f = \tilde{m}/\ell\text{n}(1+\tilde{Y}_{2,\infty}) \quad , \quad (3.57)$$

$$a_{1,1}^- + a_{2,1}^- = 0 \quad \text{or} \quad a_{2,1}^- = -a_{1,1}^- \quad , \quad (3.58)$$

$$\phi_{2,1} = \phi_{1,1} + (\tilde{m}/\tilde{r}_f^{\,2})\xi \quad . \quad (3.59)$$

Equation (3.57) determines the flame standoff distance (flame location) for a specified mass flow rate from the burner and the concentration of the ambient reactant. Equation (3.56) has been applied in the derivation of Eqs. (3.58) and (3.59).

Next, substituting Eqs. (3.44) and Eq. (3.55) as $\xi \to -\infty$ into Eq. (3.39). to determine c_6, then substituting Eqs. (3.45) and (3.55) as $\xi \to \infty$ into the resulting equation, we have

$$a_{1,1}^+ = -(a_{T,1}^+/g_0^+)\,[(g_0^+)^2 + 2\Lambda_R]^{1/2} \quad . \quad (3.60)$$

Equation (3.30) has been applied in the derivation of Eq. (3.60). Finally, substituting Eqs. (3.42) and (3.53) into Eq. (3.38). to determine c_4 and c_5, then substituting Eqs. (3.43) and (3.54) into the resulting equation, we obtain

$$[(g_0^-)^2+2\Lambda_R]^{1/2}+[(g_0^+)^2+2\Lambda_R]^{1/2}=\tilde{m}/\tilde{r}_f^{\,2} \quad , \tag{3.61}$$

$$a_{1,1}^-=(\tilde{T}_{b,1}/g_0^-)\exp(\tilde{m})[(g_0^-)^2+2\Lambda_R]^{1/2} \quad , \tag{3.62}$$

$$\phi_{1,1}=\theta_1-[(g_0^+)^2+2\Lambda_R]^{1/2}\xi \quad . \tag{3.63}$$

Equation (3.61) determines the leading order flame temperature in the presence of radiation, which is the flame temperature when the reaction rate is infinitely fast. In the adiabatic limit, $\Lambda_R=0$, Eq. (3.61) is reduced to the adiabatic flame temperature, given by

$$\tilde{T}_{ad}=1+\tilde{T}_0-(1+\tilde{T}_0-\tilde{T}_\infty)/(1+\tilde{Y}_{O,\infty}) \quad . \tag{3.61a}$$

Equations (3.57) and (3.60) have been applied in the derivation of Eq. (3.62) and (3.63). Substitution of Eqs. (3.61) and (3.63) into Eq. (3.59) changes the dependence of $\phi_{2,1}$ on θ_1 as

$$\phi_{2,1}=\theta_1+[(g_0^-)^2+2\Lambda_R]^{1/2}\xi \quad . \tag{3.64}$$

The problem is now considered solved and the result is summarized in the following. For the leading order terms, the flame location and leading order flame temperature are determined by Eqs. (3.57) and (3.61). The solution also includes a second order, nonlinear ordinary differential equation

$$d^2\theta_1/d\xi^2=\Lambda_K\,\phi_{1,1}\,\phi_{2,1}\exp(-\theta_1) \tag{3.35}$$

where $\phi_{1,1}$ and $\phi_{2,1}$ are given by

$$\phi_{1,1} = \theta_1 - [(g_0^+)^2 + 2\Lambda_R]^{1/2}\xi \quad , \tag{3.63}$$

$$\phi_{2,1} = \theta_1 + [(g_0^-)^2 + 2\Lambda_R]^{1/2}\xi \quad , \tag{3.64}$$

which needs to be solved numerically subjecting to the matching conditions in Eqs. (3.53) and (3.54), with Eq. (3.57) applied,

$$\theta_1(\xi \to -\infty) = -\{(\tilde{T}_{b,1}/g_0^-)[e^{\tilde{m}}/(1+\tilde{Y}_{2,\infty})] + \xi\}[(g_0^-)^2 + 2\Lambda_R]^{1/2} \quad , \tag{3.65}$$

$$\theta_1(\xi \to \infty) = -\{(a_{T,1}^+/g_0^+)[\tilde{Y}_{2,\infty}/(1+\tilde{Y}_{2,\infty})] - \xi\}[(g_0^+)^2 + 2\Lambda_R]^{1/2} \quad . \tag{3.66}$$

The numerical solution determines the constants $\tilde{T}_{b,1}$ and $a_{T,1}^+$, and the extinction state. The solutions of $\tilde{T}_{b,1}$ and $a_{T,1}^+$ in turn provide the reduction of flame temperature because of the finite rate radiative heat loss and kinetics,

$$\delta\tilde{T}_2^+(\tilde{r}_f) + \varepsilon\tilde{T}_1^+(\tilde{r}_f) + \ldots = \delta a_{T,2}^+[1-\exp(-\tilde{m}/\tilde{r}_f)] + \varepsilon a_{T,1}^+[1-\exp(-\tilde{m}/\tilde{r}_f)] + \ldots \quad , \tag{3.67}$$

where $a_{T,2}^+$ is expressed in Eq. (3.52), and the leakage of the burner reactant across the flame, is represented by

$$\tilde{Y}_{1,L} = \tilde{Y}_{1,1}^+(\tilde{r}_f) = a_{1,1}^+[1-\exp(-\tilde{m}/\tilde{r}_f)] \quad . \tag{3.68}$$

With the application of Eqs. (3.57) and (3.60), Eq. (3.68) can be re-arranged to

$$\tilde{Y}_{1,L} = -(a_{T,1}^+/g_0^+)[(g_0^+)^2 + 2\Lambda_R]^{1/2}\tilde{Y}_{2,\infty}/(1+\tilde{Y}_{2,\infty}) \quad . \tag{3.69}$$

Conversion of the Structure equation to Liñán's form

To simplify the numerical work, the equation system (3.35), (3.63) – (3.66) is converted to that of Liñán in his diffusion flame regime [4]. The conversion is performed by introducing a new independent variable $\bar{\xi}$, a new independent variable $\bar{\theta}$ and a

parameter γ as

$$\bar{\xi} = \alpha^{1/3}[\tilde{m}/(2\tilde{r}_{f,S}{}^2)]\xi \quad , \tag{3.70}$$

$$\bar{\theta} = \alpha^{1/3}\langle \theta_1 + \{[(g_0^-)^2 + 2\Lambda_R]^{1/2} - [(g_0^+)^2 + 2\Lambda_R]^{1/2}\}\xi/2\rangle \quad , \tag{3.71}$$

$$\gamma = (2\tilde{r}_{f,S}{}^2/\tilde{m})[(g_0^+)^2 + 2\Lambda_R]^{1/2} - 1 \quad , \tag{3.72}$$

where

$$\alpha = \Lambda_K(2\tilde{r}_{f,S}{}^2/\tilde{m})^2 \quad . \tag{3.73}$$

Applying Eqs. (3.70) and (3.71) to Eqs. (3.63) and (3.64), $\phi_{1,1}$ and $\phi_{2,1}$ are reduced to

$$\phi_{1,1} = \alpha^{-1/3}(\bar{\theta} - \bar{\xi}) \quad , \quad \phi_{2,1} = \alpha^{-1/3}(\bar{\theta} + \bar{\xi}) \quad . \tag{3.74}$$

Substituting Eqs. (3.70) – (3.74) into Eqs. (3.35), (3.65) and (3.66) then yields

$$d^2\bar{\theta}/d\bar{\xi}^2 = (\bar{\theta} - \bar{\xi})(\bar{\theta} + \bar{\xi})\exp[-\alpha^{-1/3}(\bar{\theta} + \gamma\bar{\xi})] \quad , \tag{3.75}$$

$$\bar{\theta}(\bar{\xi} \to -\infty) = -\alpha^{1/3}(\tilde{T}_{b,1}/g_0^-)[e^{\tilde{m}}/(1 + \tilde{Y}_{2,\infty})][(g_0^-)^2 + 2\Lambda_R]^{1/2} - \bar{\xi} \quad , \tag{3.76}$$

$$\bar{\theta}(\bar{\xi} \to \infty) = -\alpha^{1/3}(a_{T,1}^+/g_0^+)[\tilde{Y}_{2,\infty}/(1 + \tilde{Y}_{2,\infty})][(g_0^+)^2 + 2\Lambda_R]^{1/2} + \bar{\xi} \quad . \tag{3.77}$$

The equation (3.75) will be solved by a fourth order Runge-Kutta method.

Rescaling

The reference quantities used to nondimensionalize the variables and parameters in Chapter 2 are different for different flames, so the same numerical value for each solution describes different actual results among these flames. Comparisons among the four flames using the parameters introduced in Chapter 2 might be ambiguous and misleading. To avoid controversies in the discussion of results, the parameters are rescaled by means of absolute parameters that are independent of the flow conditions.

The rescaling is performed by first defining the heat of combustion per unit mass of the fuel, q_F, as the reference heat of combustion such that $\overline{T} = c_p T / q_F$, $\overline{Y}_{O,\infty}$ as the reference mass fraction and the adiabatic flame temperature, $\overline{T}_{ad} = 1 + \overline{T}_0 - (1 + \overline{T}_0 - \overline{T}_\infty)(1 + \overline{Y}_{O,\infty})^{-1}$, as the reference temperature. Designating properties nondimensionalized by these reference quantities by superscript "–", we can define the other parameters as

$$\overline{D}a_K = \frac{B_K \nu_O W_O \rho^2 c_p r_b^2}{\lambda_g} \quad , \quad \overline{D}a_R = \frac{B_R c_p r_b^2}{q_F \lambda_g} \quad , \quad \overline{Y}_1 = Y_1 \quad , \quad \overline{Y}_2 = \frac{\nu_F W_F}{\nu_2 W_2} Y_2 \quad ,$$

$$\overline{E}_K = \frac{c_p E_K}{q_F} \quad , \quad \overline{E}_R = \frac{c_p E_R}{q_F} \quad , \quad \overline{\delta} = \overline{T}_{ad}^2 / \overline{E}_R \quad , \quad \overline{\varepsilon} = \overline{T}_{ad}^2 / \overline{E}_K \quad ,$$

$$\overline{\Lambda}_K = \overline{\varepsilon}^3 \overline{D}a_K \exp(-\overline{E}_K / \overline{T}_{ad}) \quad , \quad \overline{\Lambda}_R = \overline{\delta}\, \overline{D}a_R \exp(-\overline{E}_R / \overline{T}_{ad}) \quad .$$

With these rescaled parameters, the parameters required to present the results can be rescaled to

$$\Lambda_K = \overline{\Lambda}_K (\overline{T}_f / \overline{T}_{ad})^6 (q_F / q_1)^3 [\nu_2 w_2 / (\nu_O w_O)] Y_{1,0}^{-2} \exp[\overline{E}_K (\overline{T}_{ad}^{-1} - \overline{T}_f^{-1})] \quad , \tag{3.78}$$

$$\Lambda_R = \overline{\Lambda}_R (\overline{T}_f / \overline{T}_{ad})^2 [q_F / (q_1 Y_{1,0})]^2 \exp[\overline{E}_R (\overline{T}_{ad}^{-1} - \overline{T}_f^{-1})] \quad , \tag{3.79}$$

$$\overline{Y}_{1,L} = [q_F / (q_1 Y_{1,0})] (\overline{T}_f / \overline{T}_{ad})^2 \tilde{Y}_{1,L} \quad . \tag{3.80}$$

Chapter 4

Results and Discussions

To exhibit the salient feature of this study, numerical calculations were performed using the following thermal physical data:

$$T_0 = T_\infty = 298\text{K} \quad , \quad q_F = 47160 \text{ J/g} \quad , \quad c_p = 1.3232 \text{ J/(g·K)} \quad ,$$

$$\lambda_g = 0.0012043 \text{ W/(cm·K)} \quad , \quad E_K = 24000 \text{ K} \quad , \quad E_R = 8000 \text{ K} \quad ,$$

$$\nu_F = 1 \quad , \quad \nu_O = 3 \quad , \quad W_F = 28 \text{ g/mole} \quad , \quad W_O = 32 \text{ g/mole} \quad .$$

These data closely represent the burning of ethylene in air. The burner size is taken to be $r_b = 0.3175$ cm, the size of the burner used in the experiments performed by the group at the NASA Glenn Research Center. A FORTRAN program was developed to solve Eq. (3.75) subject to the boundary conditions in Eqs. (3.76) and (3.77).

As mentioned in Chapter 1, both the flow direction and flame structure can be independently controlled for the spherical burner stabilized flame. Using the ethylene/air flame as the model flame, four limiting cases similar to those of Liu et al. [34] and Sunderland et al. [35] were studied. These flames are (A) fuel (ethylene) issuing into air, (B) diluted fuel issuing into oxygen, (C) air issuing into fuel and (D) oxygen issuing into diluted fuel. Flame A is a common flame that we are familiar with and Flame B is obtained by extracting all the inert from the air and diverting it to the fuel. Flame C is an inversion of flame A by issuing air from the burner into an ambient filled with the fuel, and Flame D is the inversion of Flame B. All these flames have the same stoichiometric ratio and, hence, the same adiabatic flame temperature.

1. Temperature Distribution

Discussions on the effects of radiative heat loss begin with its effect on the leading order flame temperature T_f, which can be calculated from Eq. (3.61) with $\tilde{r}_f$ given by Eq. (3.57) for specified values of the mass flow rate m and radiation intensity $\overline{\Lambda}_R$. And the results for the four flames are shown in Figs. 1 – 4. These figures show that

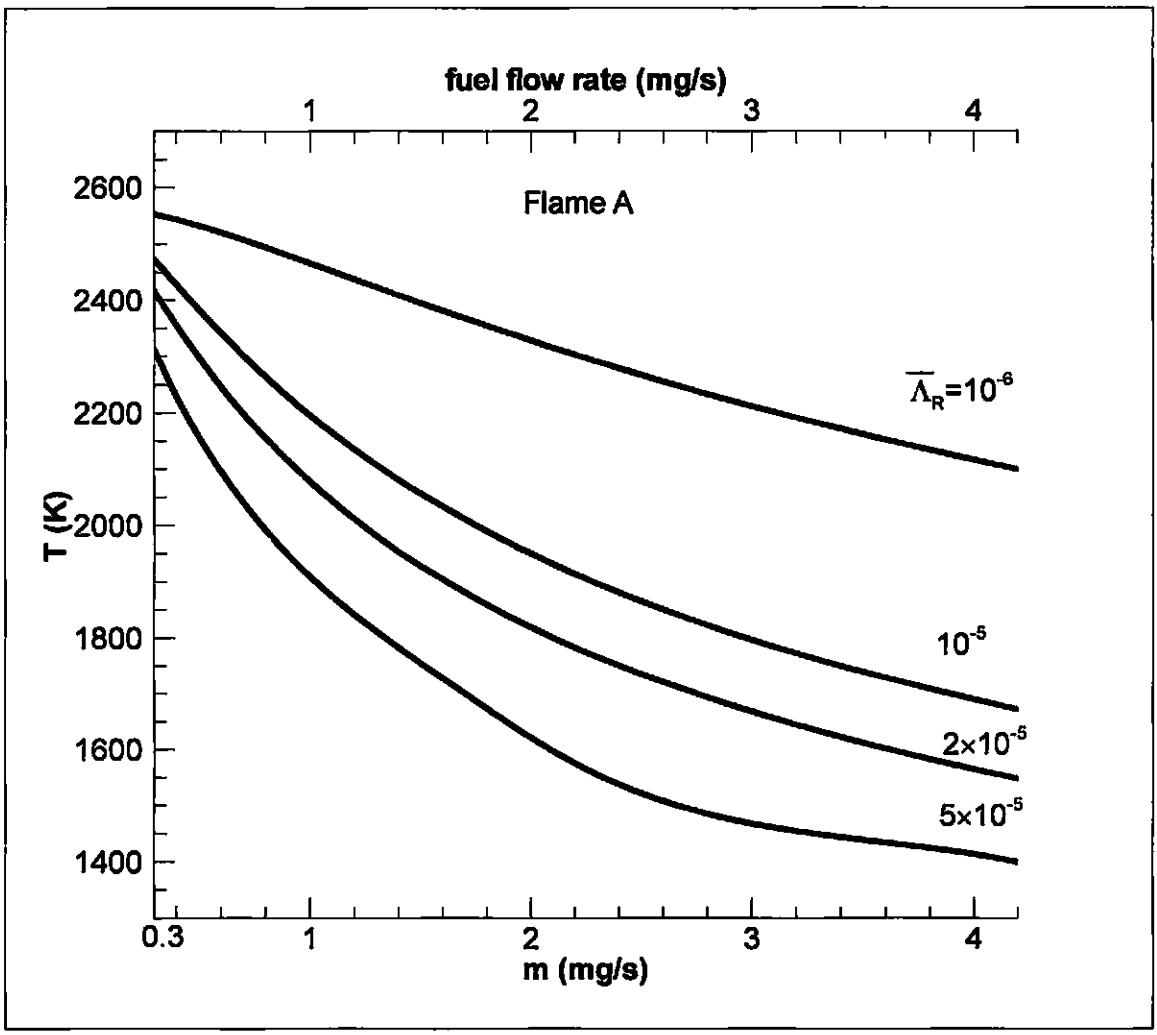

Figure 4.1 Variation of the leading order flame temperature versus the mass flowrate and radiation intensity for Flame A.

for a given value of m, the flame temperature decreases with increasing $\overline{\Lambda}_R$, as should be because a higher heat loss intensity leads to a higher heat loss rate. The flame temperature also decreases by increasing the mass flow rate while keeping $\overline{\Lambda}_R$ fixed. This is a result of the increased flame size. As is known, radiative heat loss is a volumetric loss mechanism. The rate of heat loss increases when the volume of the heat loss region increases. Equation (3.57) shows that the flame radius varies linearly with

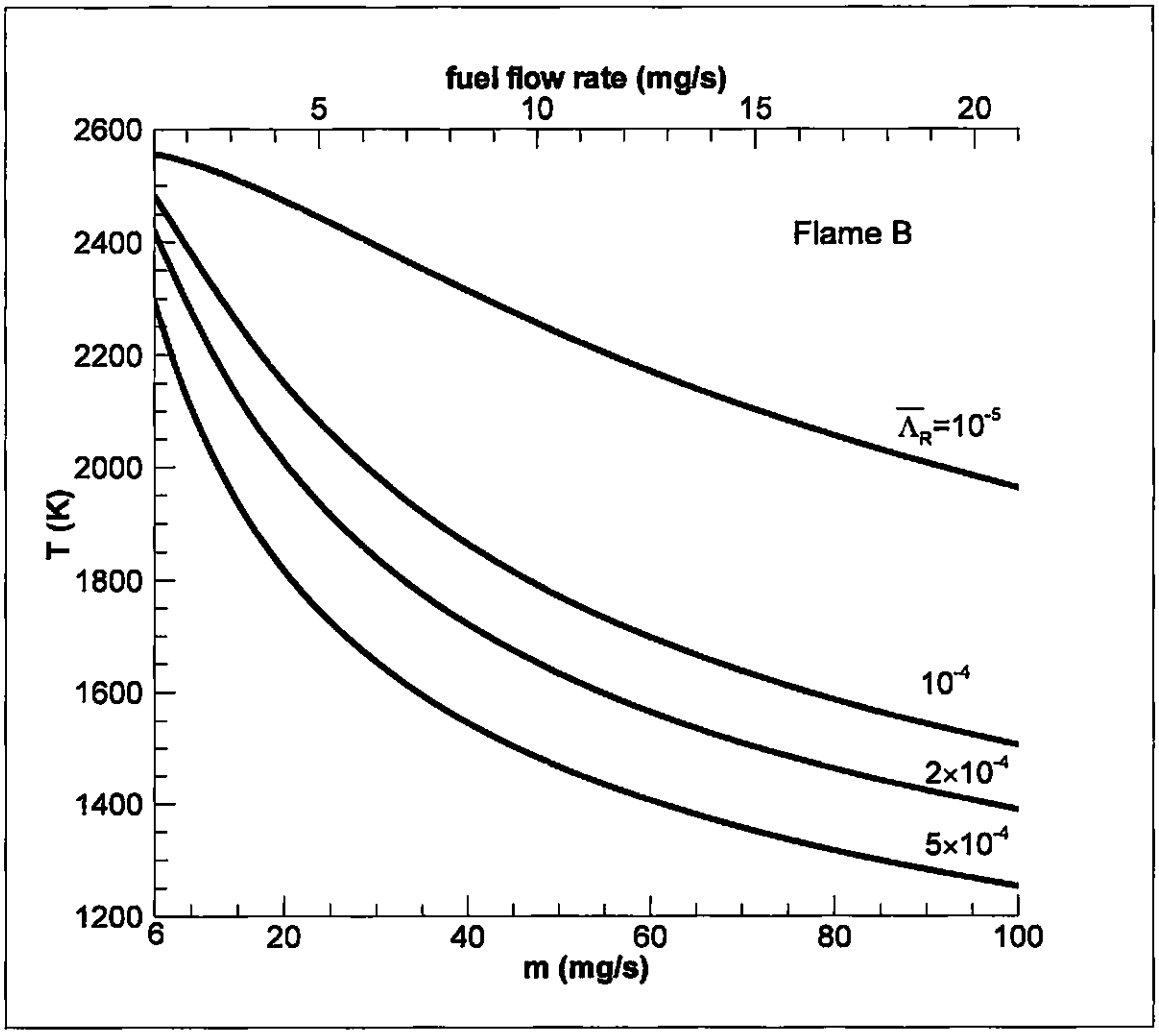

Figure 4.2 Variation of the leading order flame temperature versus the mass flowrate and radiation intensity for Flame B.

the mass flow rate. Since the volume of the radiation roughly depends on the area of the flame sheet ($4\pi r_f^2$) and the thickness of the radiation region, which is practically independent of the flow rate, the heat loss rate thus varies with m squared. Therefore, by increasing mass flow rate, the heat generation rate increases with m linearly while the heat loss rate increases with m^2, and the flame temperature decreases. These behaviors are qualitatively similar for all four flames.

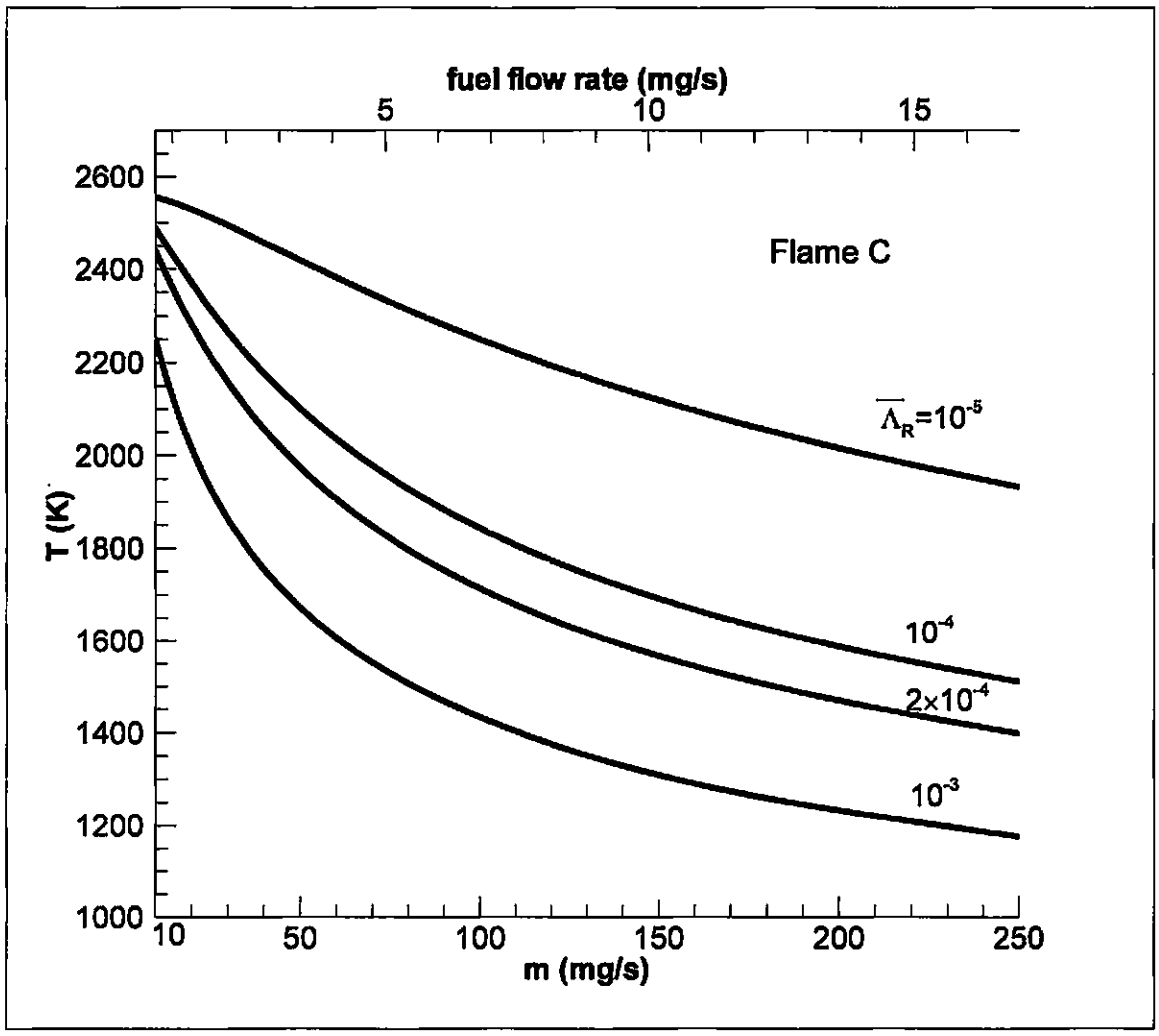

Figure 4.3 Variation of the leading order flame temperature versus the mass flowrate and radiation intensity for Flame C.

Comparison on the results of the four flames shows that the effect of radiation is stronger on Flames A and D than that on Flames B and C. Because the inert is flowing with the burner reactant for Flames B and C, the mass fraction of the burner reactant is low. As a result, the flame is smaller (comparing to Flames A and D) and the volume of the radiation region is smaller. Consequently, the rate of heat loss is lower and its effect is weaker.

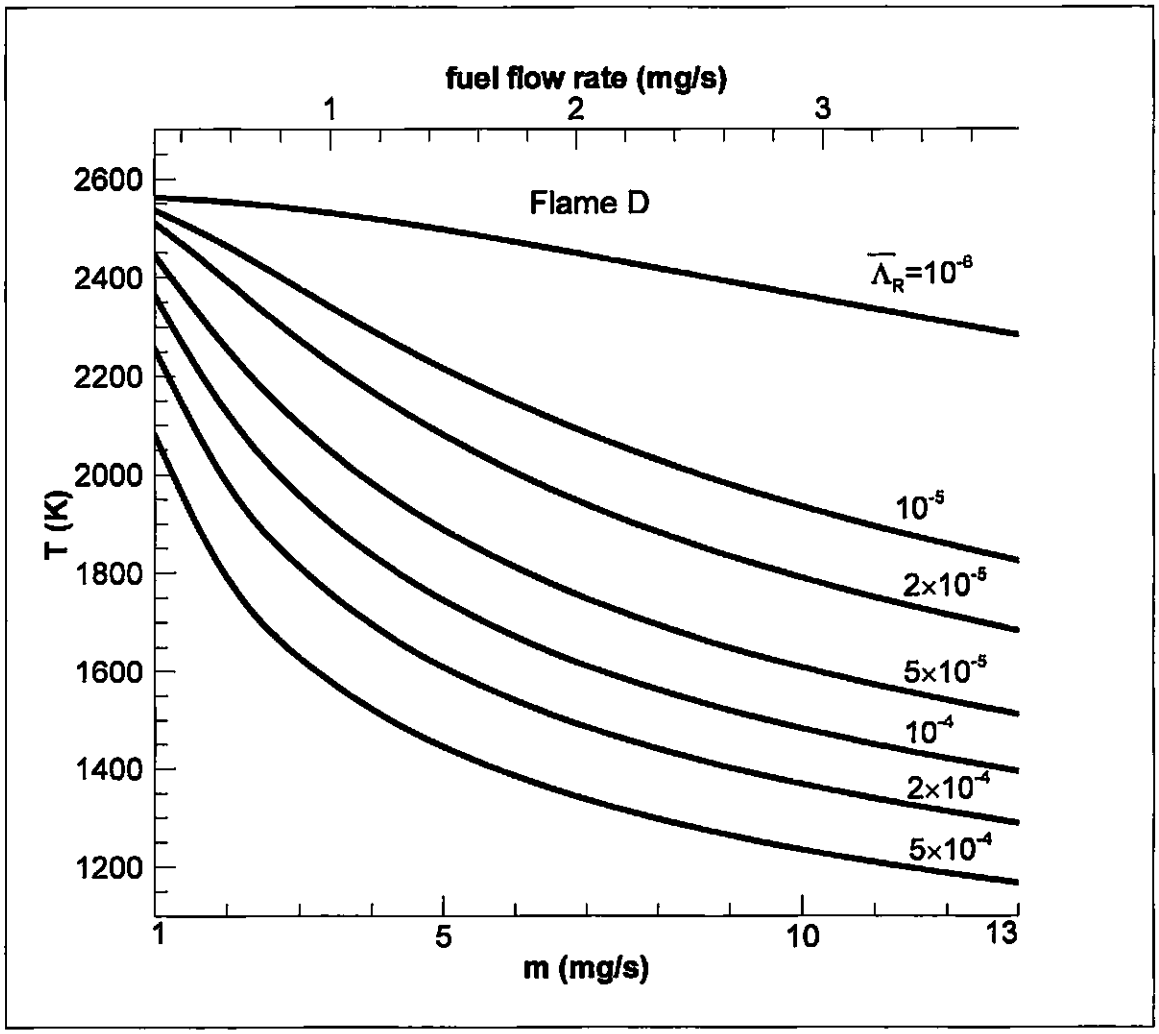

Figure 4.4 Variation of the leading order flame temperature versus the mass flowrate and radiation intensity for Flame D.

2. Kinetic Extinction Limit

Flame extinction is not observable in the leading order flame temperature presented in Figs. 4.1 – 4.4 because the temperature is obtained by assuming the reaction rate to be infinitely fast. When the reaction rate, represented by the reduced Damköhler number $\overline{\Lambda}_K$, is finite, flame extinction occurs when the reaction rate becomes too slow. The extinction phenomenon can be exhibited by solving Eq. (3.75) numerically subject to Eqs. (3.76) and (3.77). The results are presented by plotting the parameter representing the leakage of the burner reactant, $\overline{Y}_{1,L}$, versus $\overline{\Lambda}_K$, for a fixed mass flowrate and selected values of $\overline{\Lambda}_R$. Figures 4.5 – 4.8 show the results for Flames A – D using the same fuel consumption rate of m = 2 mg/s, which yields different mass flowrates of 2, 24.57, 29.43 and 6.86 mg/s, respectively for the four flames. The adiabatic limit, given by the curve by setting $\overline{\Lambda}_R = 0$, is also plotted for comparison. These figures show that for a specified radiation intensity $\overline{\Lambda}_R$, there are two solutions for a given value of $\overline{\Lambda}_K$ when it is higher than a minimum value and there is no solution when it is below this critical value. The minimum value of $\overline{\Lambda}_K$ below which the solution fails to exist is identified as the extinction state. The lower branch that shows a decrease of $\overline{Y}_{1,L}$ with increasing $\overline{\Lambda}_K$, meaning that the reactant leakage is reduced when the reaction is stronger, is physically realistic. For each of the flames, the extinction Damköhler number is higher for a larger $\overline{\Lambda}_R$, showing that extinction occurs easier with stronger radiation intensity, as it should be. This extinction limit, which is induced by low reaction rate and exists even without radiative heat loss, is the well-known kinetic extinction limit.

Comparison among different flames reveals that for a same value of $\overline{\Lambda}_R$, the

leakage of burner reactant is much larger for Flames A and D than that for Flames B and C, because of their higher initial concentration. Figures 4.5 – 4.8 also show that in the adiabatic limit or at low radiation intensities, the flame is stronger (more difficult to extinguish) when the mass flow rate is smaller. That is, Flame A is the most difficult to extinguish, followed by Flames D and B, while Flame C is the easiest to extinguish. When the radiation intensity is low, its effect on flame behavior is weaker and the burning intensity is primarily controlled by the residence time if the kinetic data are kept the same.

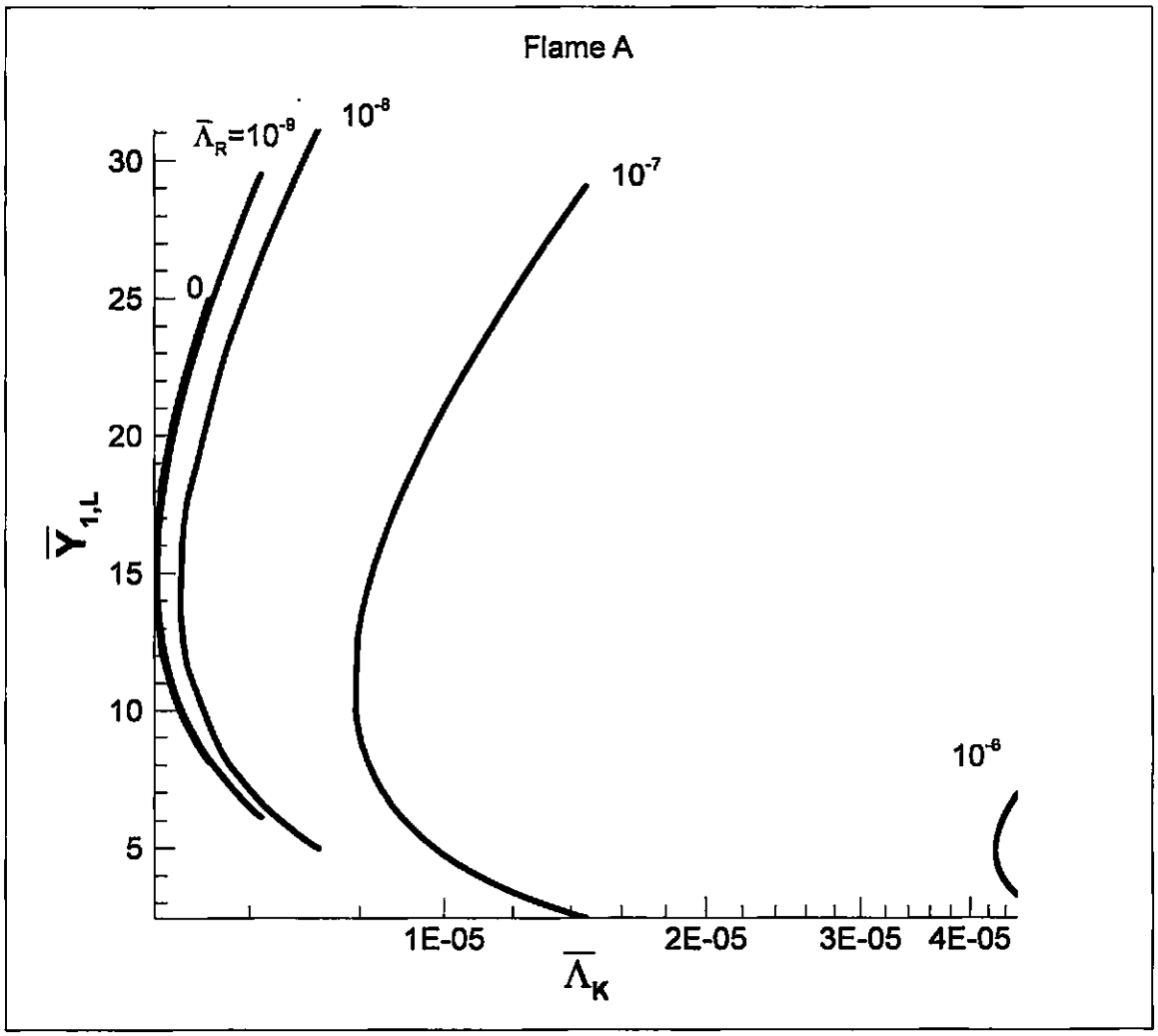

Figure 4.5. Effects of radiative heat loss on reactant leakage and flame extinction for Flame A with the fuel consumption rate kept at 2 mg/s.

A lower mass flow rate yields a longer residence time for the burner reactant to pass through the reaction region and the reaction to occur. In addition to the low mass flowrate, a larger flame size for Flames A and D further increases their residence times. Because the range of $\overline{\Lambda}_K$ spread to a wide range in response to the variation of $\overline{\Lambda}_R$, it is not clear whether the same conclusion is true when the radiation is strong.

To exhibit the extinction characteristics at strong radiation intensities, results

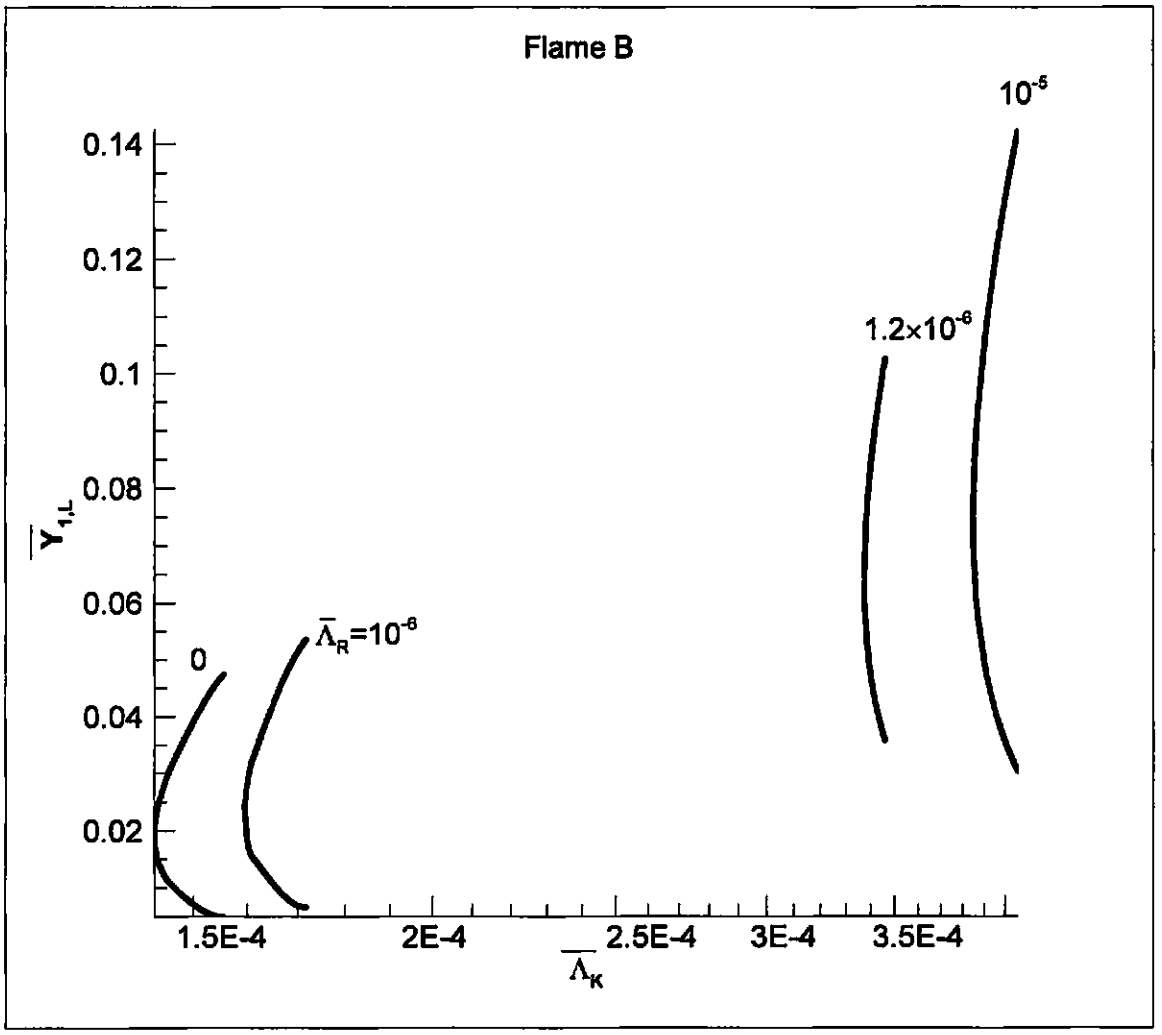

Figure 4.6. Effects of radiative heat loss on reactant leakage and flame extinction for Flame B with the fuel consumption rate kept at 2 mg/s.

of two radiation intensities, $\overline{\Lambda}_R = 10^{-5}$ and 10^{-6}, for Flames A and B are plotted in Fig. 9. It is shown that when $\overline{\Lambda}_R = 10^{-6}$, the extinction is controlled by the residence time as shown in Figs. 4.1 – 4.4. However, when $\overline{\Lambda}_R = 10^{-5}$, the qualitative behavior is reversed. That is, the flame with higher mass flowrate (Flame B) becomes more difficult to extinguish. This shows that when the radiation intensity is sufficiently strong, the effect of radiation becomes significant and is comparable to or even dominate over that

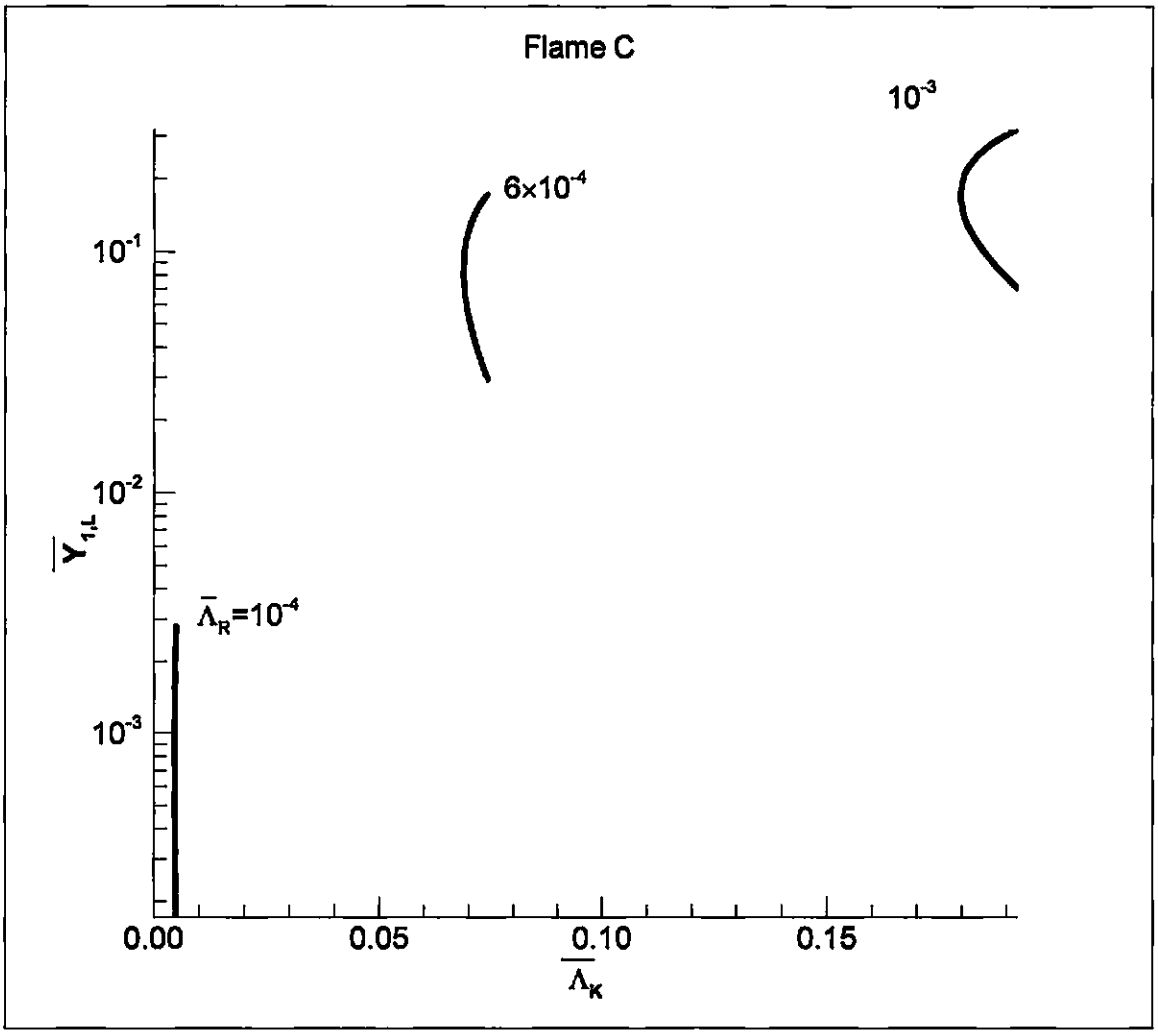

Figure 4.7. Effects of radiative heat loss on reactant leakage and flame extinction for Flame C with the fuel consumption rate kept at 2 mg/s.

of residence time. Because the flame size of Flame A is much larger than that of Flame B, the volume of the radiation region is much broader such that the heat loss rate is greater. A stronger heat loss yields a larger reduction in flame temperature, which makes the flame weaker and easier to extinguish. Similar results are observed when other flames are compared. Therefore, when a flame suffers stronger radiative heat loss, the extinction state is characterized by both the residence time and the energy loss.

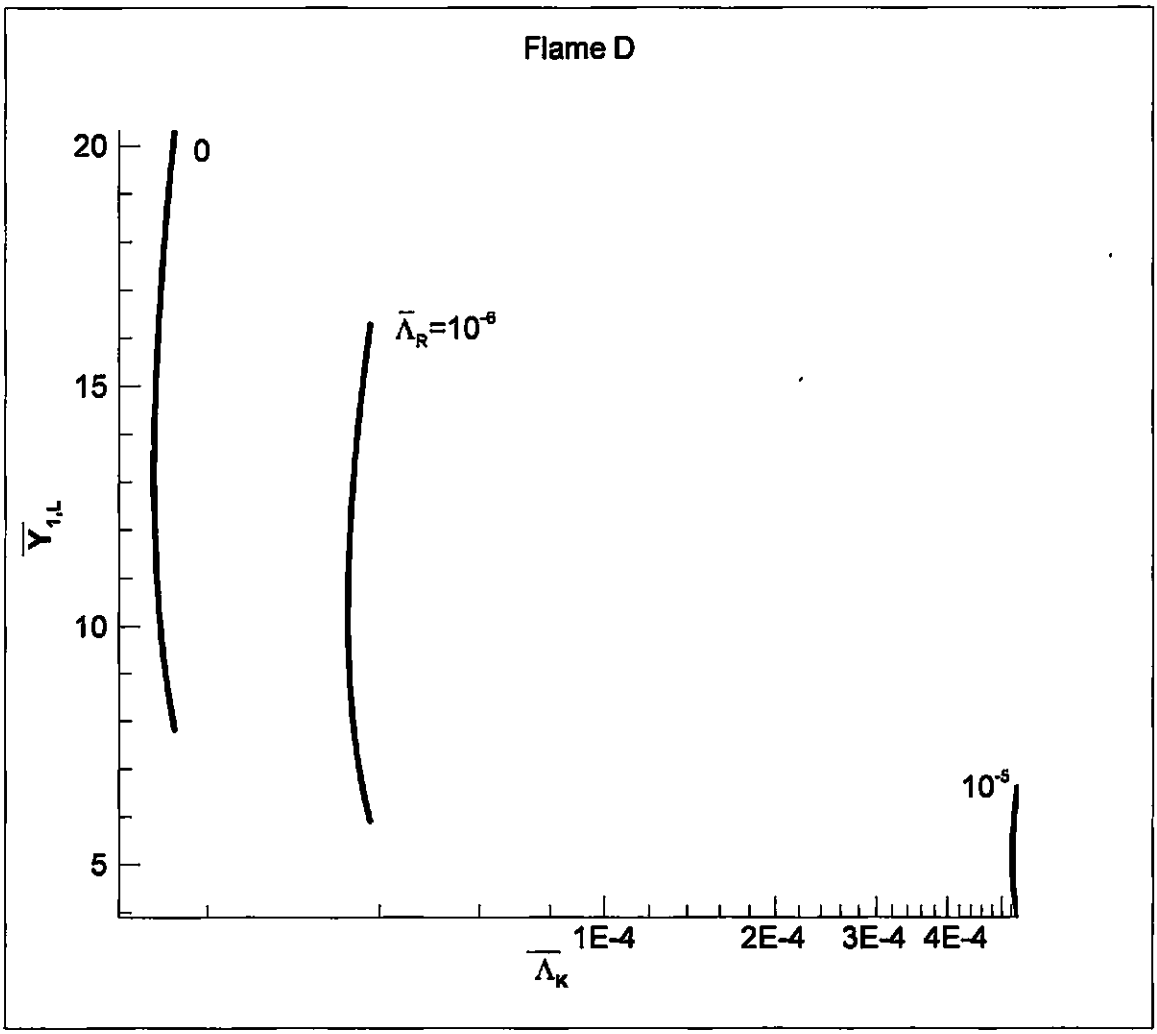

Figure 4.8 Effects of radiative heat loss on reactant leakage and flame extinction for Flame D with the fuel consumption rate kept at 2 mg/s.

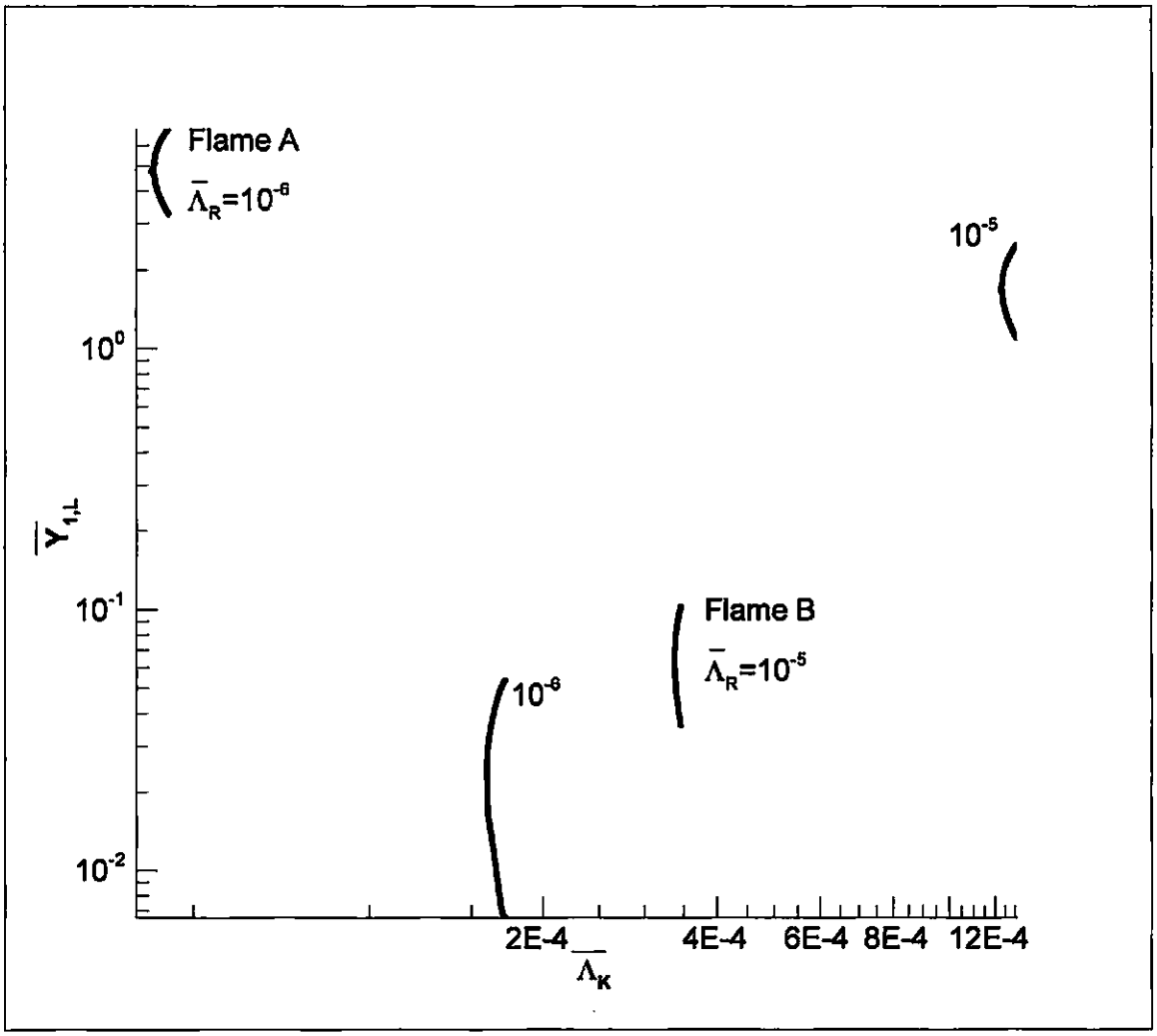

Figure 4.9 Comparison of the extinction state between Flames A and B with low and high radiation intensities.

3. Kinetic and Radiative Extinction Limits

The discussion is continued with varying the mass flow rate while keeping the radiation intensity fixed. In Figs. 4.10 – 4.13, the leakage of the burner reactant, $\bar{Y}_{1,L}$, is plotted versus the mass flowrate for some values of $\bar{\Lambda}_K$ for a selected value of $\bar{\Lambda}_R$. The value of $\bar{\Lambda}_R$ is chosen such that the results can be presented most clearly and is different for different flames. These figures show that for each selected value of $\bar{\Lambda}_K$, there exists a

minimum value of m below which there is no solution, as in Figs. 4.5 – 4.8, and this critical m represents the kinetic extinction state. For values of m greater than the kinetic extinction limit, there are two solutions corresponding to each m, between them the lower branch is the physically realistic solution. Contrary to Figs. 4.5 – 4.8 that the reactant leakage continues to reduce with increasing $\overline{\Lambda}_K$, the reactant leakage first decreases and then increases by increasing m from a smaller value. Moreover, there exists a maximum

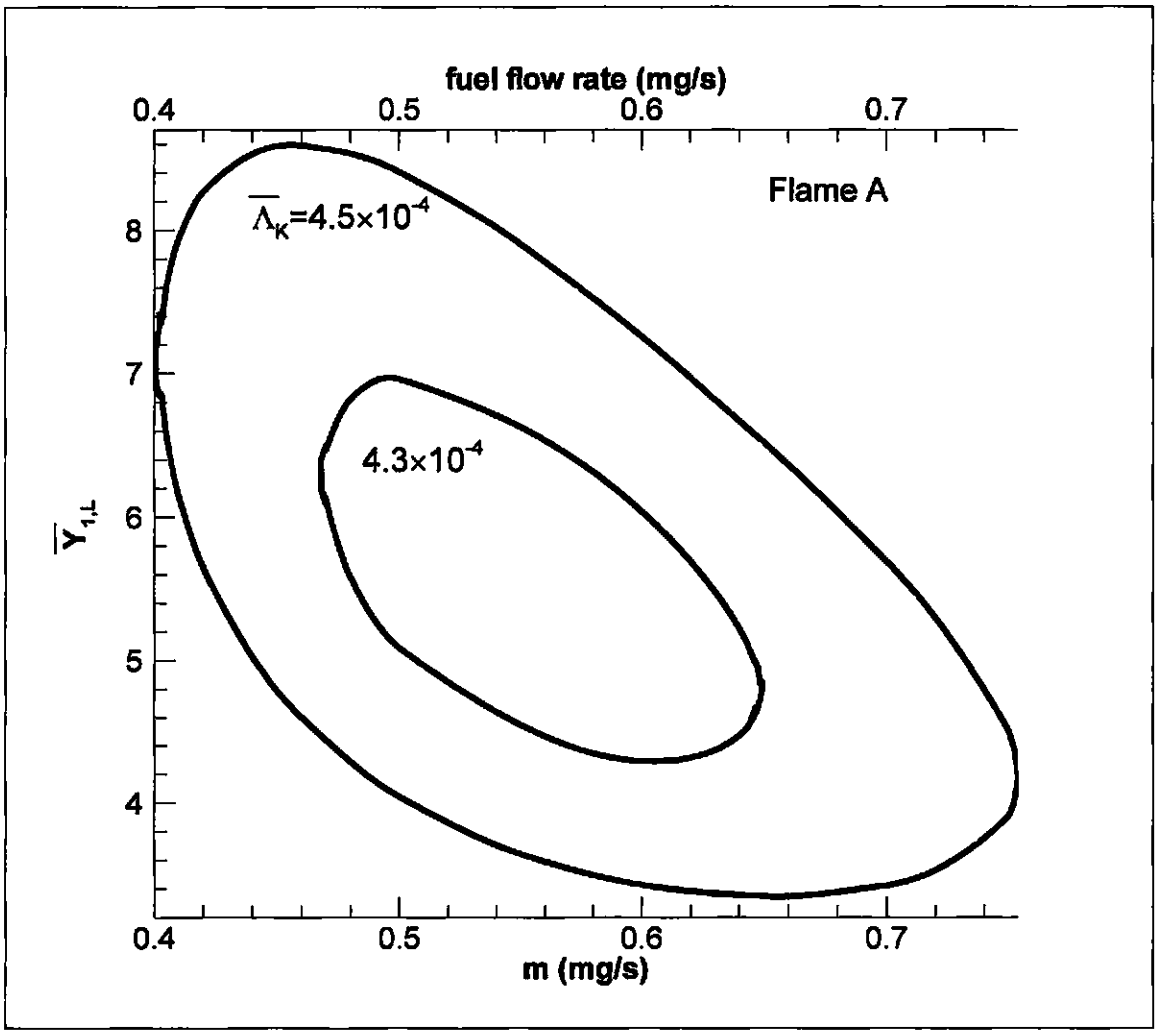

Figure 4.10 Variation of reactant leakage as a function of mass flow rate for selected values of $\overline{\Lambda}_K$. The value of $\overline{\Lambda}_R$ is 10^{-5} for Flame A.

value of m above which there is no solution either. This maximum value of m defines another extinction state, which does not exist without radiation and is the radiative extinction limit [18]. This extinction is a result of excessive heat loss caused by the increase of the flame size. Steady burning is possible only when the mass flowrate is between the two extinction limits.

As mentioned in Section 1 of this Chapter, the heat generation rate scales linearly

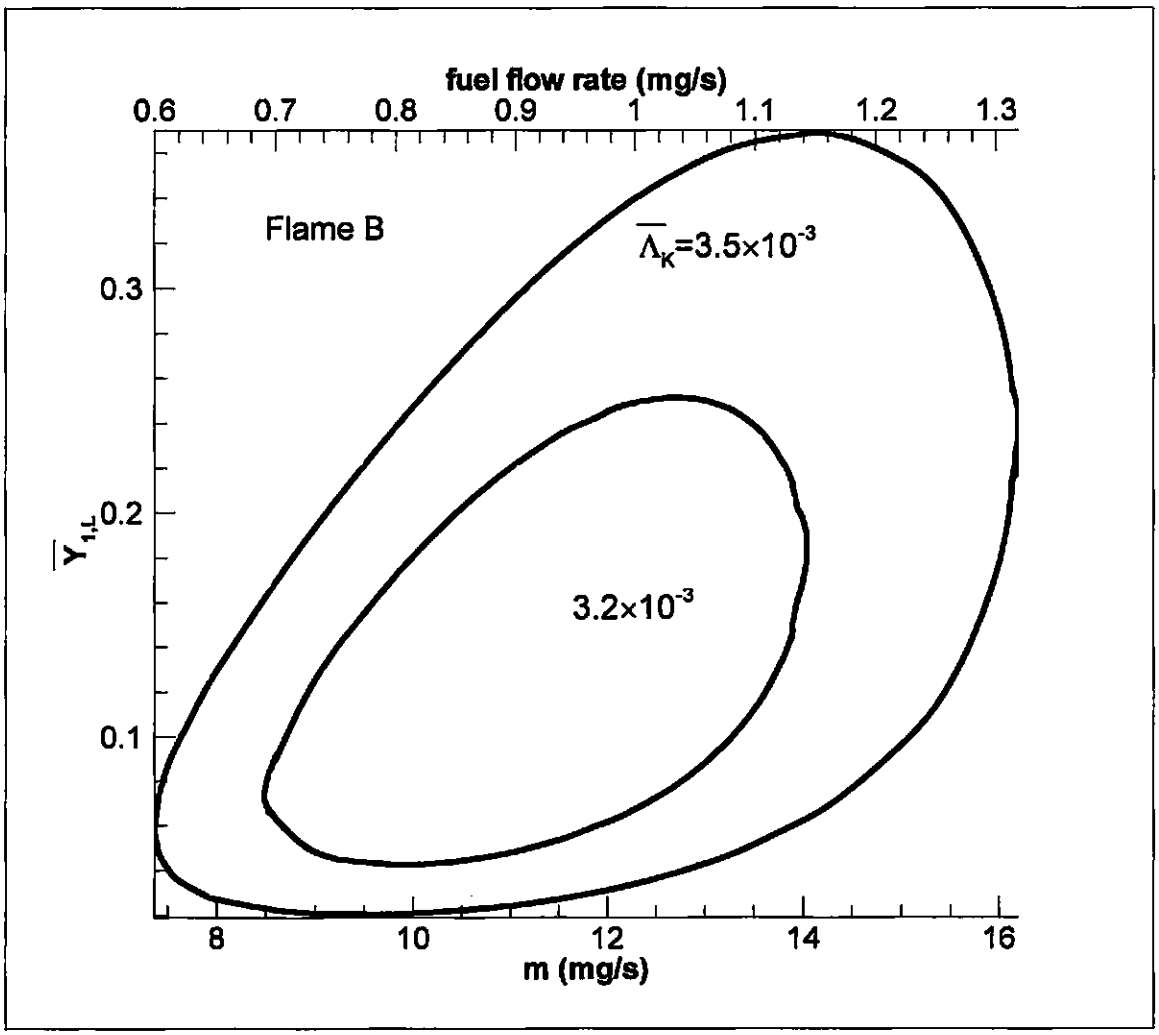

Figure 4.11 Variation of reactant leakage as a function of mass flow rate for selected values of $\overline{\Lambda}_K$. The value of $\overline{\Lambda}_R$ is 10–4 for Flames B.

with the mass flow rate m while the radiative heat loss rate scales with m^2. By increasing m, the heat loss rate increases faster than the heat generation rate so the total energy is decreased and the flame temperature is reduced. When the mass flow rate is low, the flame is small, the effect of radiation is weak and the flame behavior is controlled by the residence time. Since the residence time scales with m, the reaction is favored by increasing m such that the reactant leakage, represented by $\overline{Y}_{1,L}$, is reduced. Through

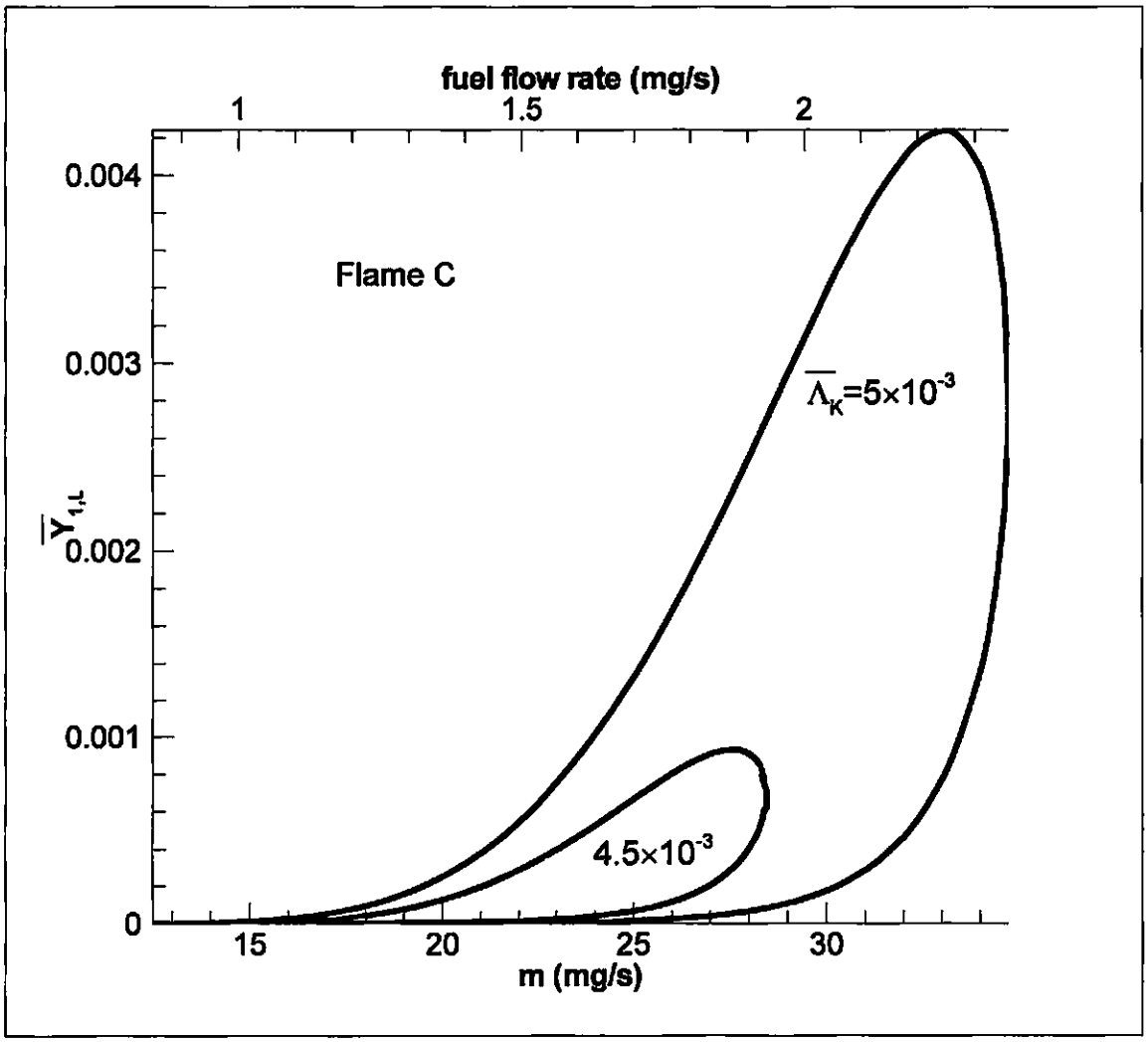

Figure 4.12 Variation of reactant leakage as a function of mass flow rate for selected values of $\overline{\Lambda}_K$. The value of $\overline{\Lambda}_R$ is 10^{-4} for Flames C.

increasing m, the flame size continues to grow and the effect of radiation becomes important. At large values of m, the negative impact of radiation dominates over the positive effect of the residence time such that the flame becomes weaker for a higher m and the reactant leakage starts to increase again. Radiative extinction limit is reached when the heat loss becomes excessive, the reaction rate becomes too slow and the flame fails to sustain itself.

Figures 4.10 – 4.13 also show that the range of m within which a steady flame

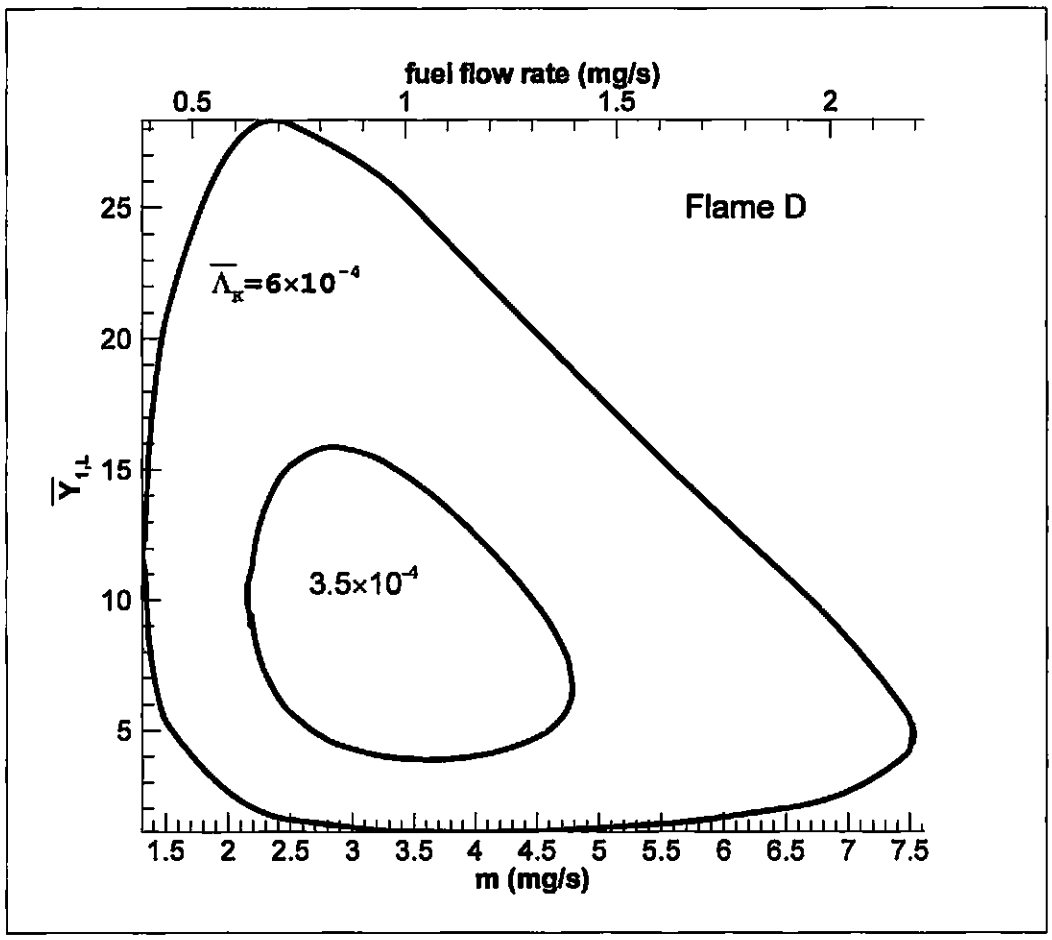

Figure 4.13 Variation of reactant leakage as a function of mass flow rate for selected values of $\overline{\Lambda}_K$. The value of $\overline{\Lambda}_R$ is 10^{-5} for Flames D.

exists become narrower with decreasing $\overline{\Lambda}_K$ because of the reduced reaction rate. As a consequence, there exists a minimum $\overline{\Lambda}_K$ below which steady burning is absolutely impossible. This minimum $\overline{\Lambda}_K$ represents the flammability limit for the specified $\overline{\Lambda}_R$. Similar results were obtained by selecting a fixed value for $\overline{\Lambda}_K$ and some values of $\overline{\Lambda}_R$. For this case, the region in which steady burning exists decreases with increasing $\overline{\Lambda}_R$, and there exists a maximum $\overline{\Lambda}_R$ above which steady burning is absolutely impossible for that specific value of $\overline{\Lambda}_K$.

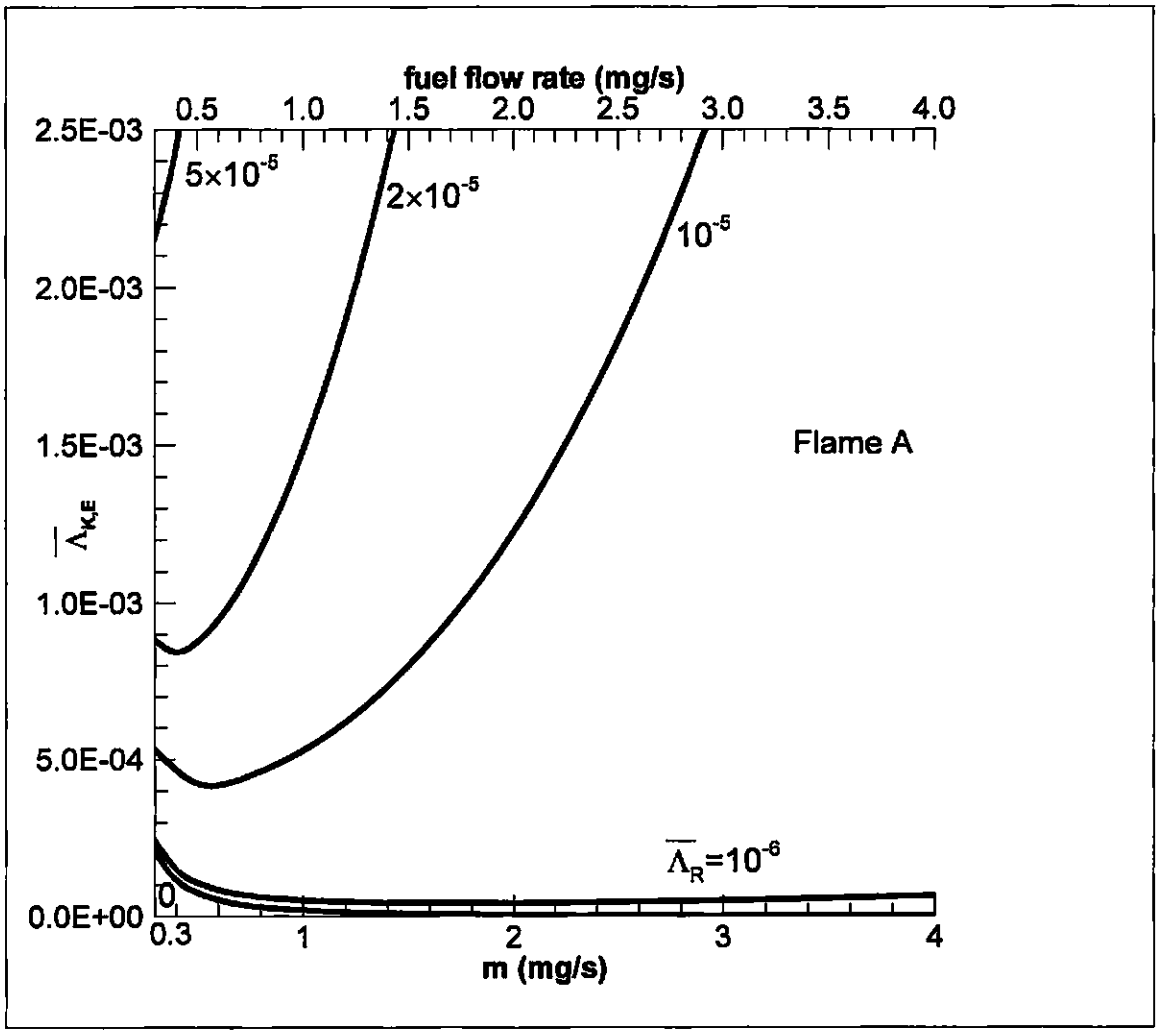

Figure 4.14 Variation of extinction Damköhler number versus the mass flow rate for specified values of $\overline{\Lambda}_R$ for Flame A.

4. Flammable Range and Flammability Limit

To further explore the results presented in Section 3, the extinction states, $\overline{\Lambda}_{K,E}$, observed in Section 3 are plotted versus the mass flow rate and radiation intensity for the four flames in Figs. 4.14 – 4.17. Results for the adiabatic flame ($\overline{\Lambda}_R = 0$) are also plotted for comparison. In these figures, the minimum value of m for all the curves is the flow rate at which the flame is located at the burner exit. If the mass flow rates fall smaller

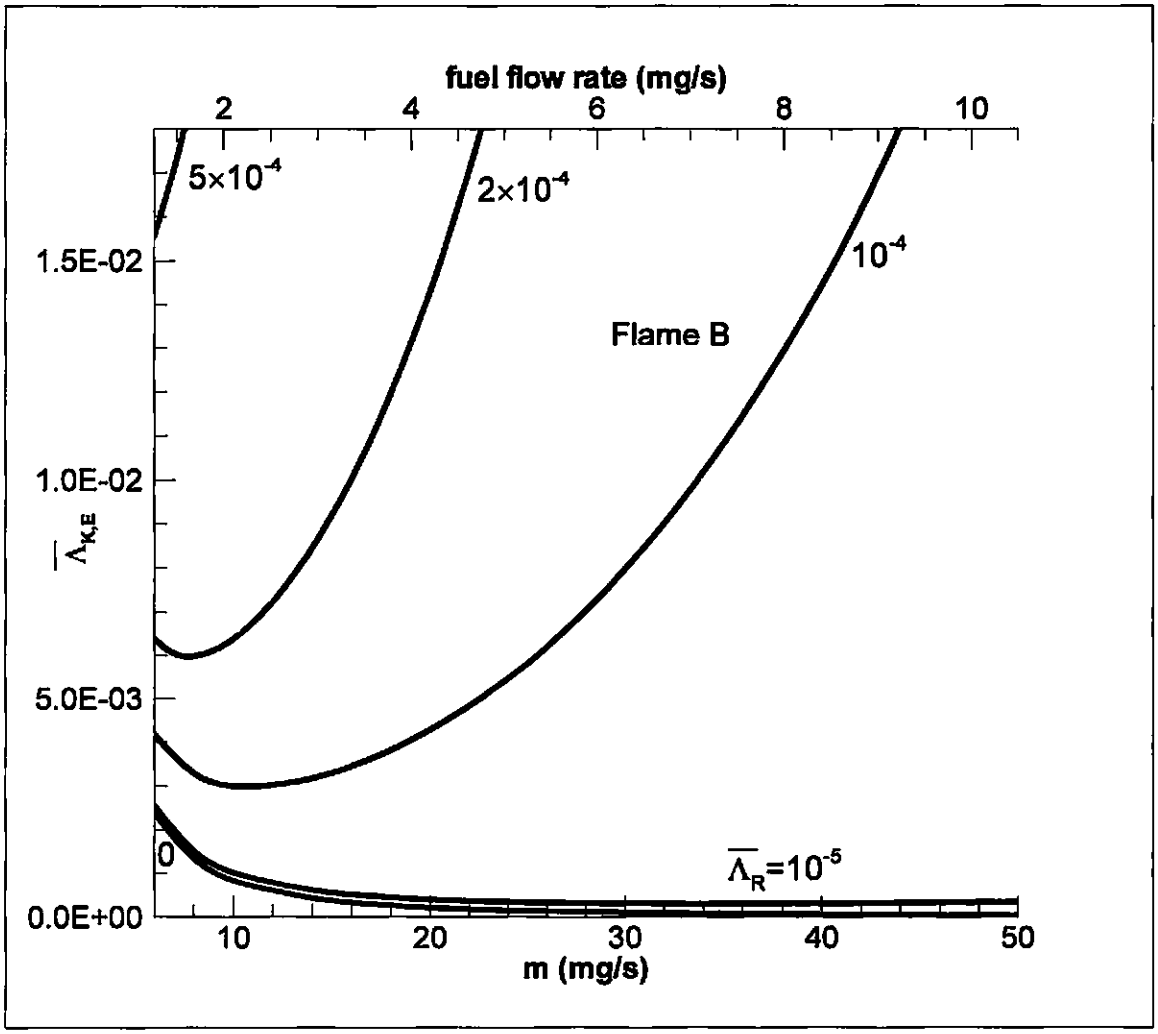

Figure 4.15 Variation of extinction Damköhler number versus the mass flow rate for specified values of $\overline{\Lambda}_R$ for Flame B.

than this minimum value, the flame would recede and locate within the burner. It would be physically unrealistic, because flame cannot be established inside the burner. For each of the cases presented, the region above each curve represents the region in which steady burning is possible, so the curve represents the boundary between the flammable and non-flammable conditions. The right branch of each curve is the radiative extinction limit and the left branch is the kinetic extinction limit. As it is known, for the adiabatic

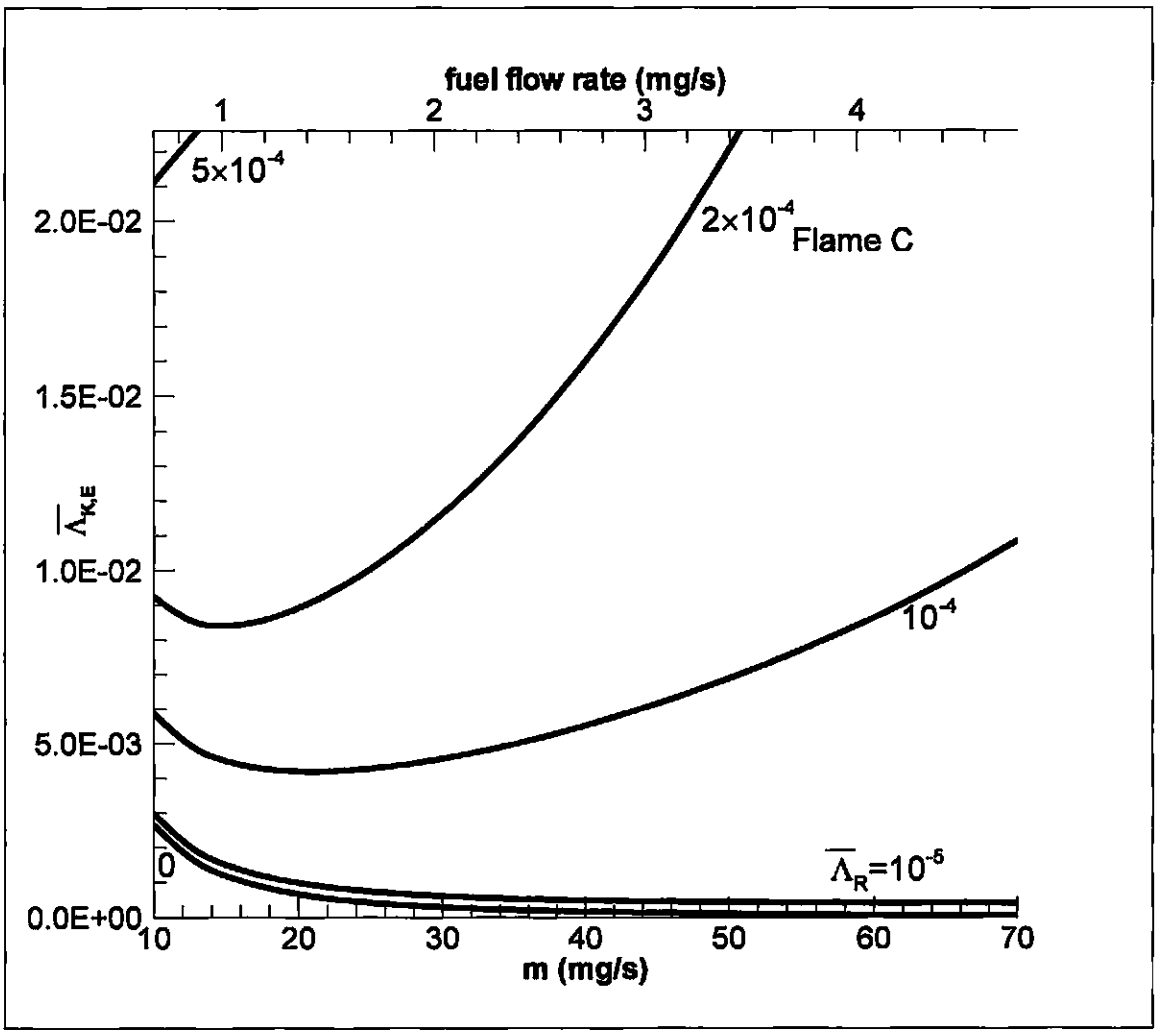

Figure 4.16 Variation of extinction Damköhler number versus the mass flow rate for specified values of $\overline{\Lambda}_R$ for Flame C.

flame, $\overline{\Lambda}_{K,E}$ decreases monotonically with increasing mass flowrate, so the kinetic extinction limit only exists. Consistent with earlier discussions, the flammable region decreases with stronger radiation (greater $\overline{\Lambda}_R$). As in Figs. 5 – 8, Figs. 14 – 17 show that the flame with longer residence time is more difficult to extinguish when the radiation is weak and that the larger flame is more easily to extinguish when the radiation is strong. The minimum value of $\overline{\Lambda}_{K,E}$ corresponding to each $\overline{\Lambda}_R$ represents the value below which steady burning is absolutely impossible and is defined as the flammability limit.

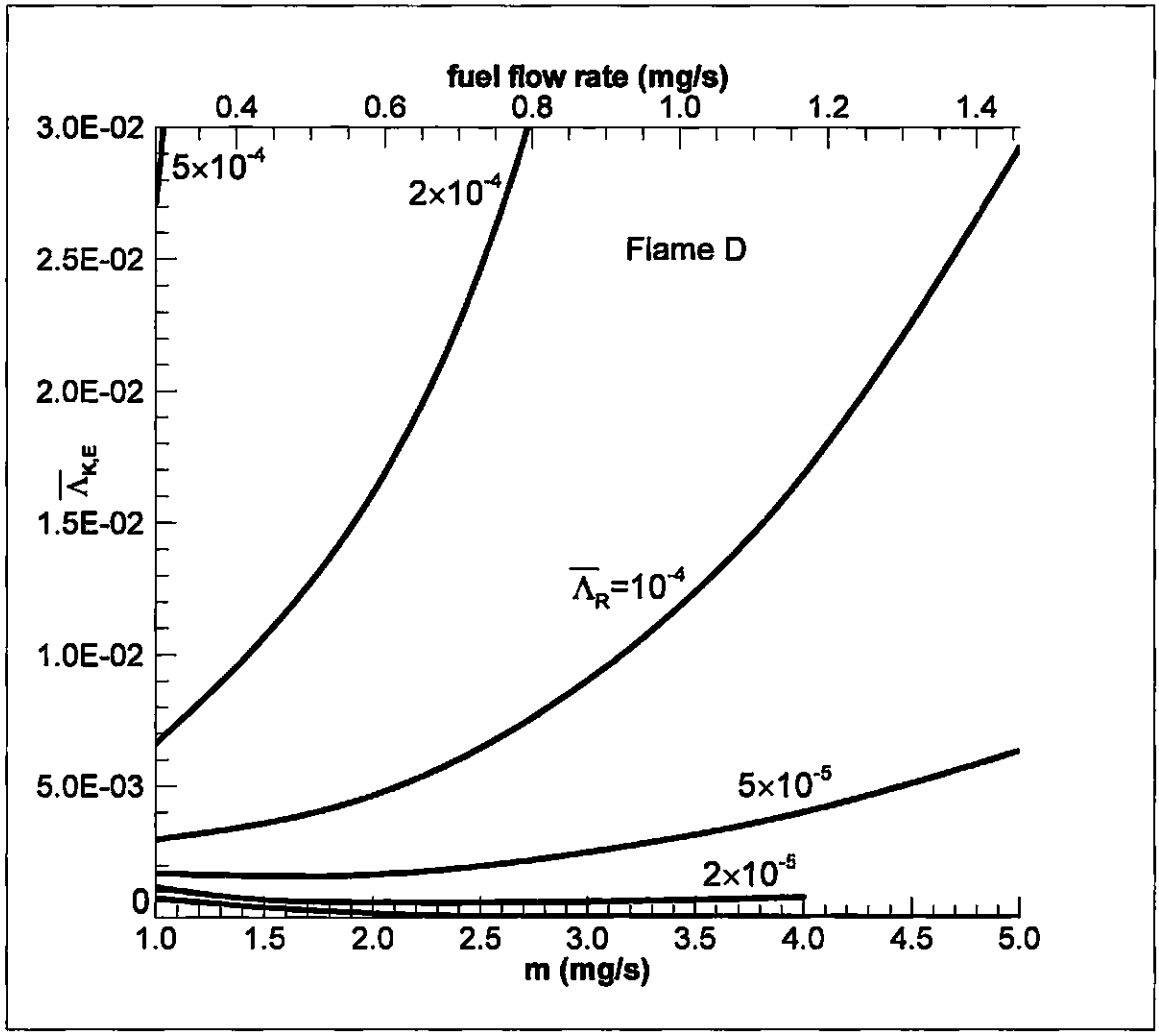

Figure 4.17 Variation of extinction Damköhler number versus the mass flow rate for specified values of $\overline{\Lambda}_R$ for Flame D.

Chapter 5

Concluding Remarks

In this study, the kinetic and radiative extinction limits as well as the flammability limit of a spherical diffusion flame stabilized by a spherical porous burner with radiative heat loss in microgravity were analyzed by activation energy asymptotics. An optically thin radiation model was adopted to describe the radiative heat loss rate. Four different flames having the same adiabatic flame temperature but different residence time, flame size, flame structure and convection direction were investigated and the results were compared. The convection direction was allowed to be varied either from the fuel to the oxidizer side by issuing a fuel flow from the burner into a quiescent oxidizing mixture or from the oxidizer to the fuel side by supplying an oxidizer flow from the burner into a fuel ambient. The flame structure can be independently controlled by supplying the inert gas (e.g. nitrogen) with either oxygen or fuel.

The major findings of the present study include:

1. From varying the radiation intensity while keeping the mass flow rate unchanged, only the kinetic extinction limit at a minimum Damköhler number exists. The extinction Damköhler number increases with increasing radiation intensity because of greater heat loss. When the heat loss is weak, the extinction characteristics are primarily controlled by the residence time and the flame with longer residence time for reaction is stronger. For flames under strong radiation intensity, the flame size, which determines the total heat loss rate, becomes

dominant and the larger flames are easier to extinguish.

2. By varying the mass flowrate (flame size) while keeping the reaction intensities unchanged, the flame temperature is reduced by increasing either the radiation intensity or the mass flowrate. For a given reaction and radiation intensity, there exist two extinction limits, a kinetic extinction limit at low flow rates and a radiative extinction limit at high flow rates. Steady burning is only possible when the flow rate falls between these two limits. For a specified reaction intensity (Damköhler number), the region in which steady burning is possible reduces with increasing radiation intensity. Consequently, there exists a maximum radiation intensity above which steady burning is not possible. The radiation intensity that yields the flammability limit is higher for a larger Damköhler number.

References

[1] http://en.wikipedia.org/wiki/Esperanza_Fire

[2] http://en.wikipedia.org/wiki/Soot

[3] Fendell, F.E.: *Ignition and extinction in combustion of initially unmixed reactants.* J. Fluid Mech. 21 (1965) 281-303.

[4] Liñán, A.: *The Asymptotic Structure of Counterflow Diffusion Flames for Large Activation Energies.* Acta Astronautica 1 (1974), 1007-1039.

[5] Law, C.K.: *Asymptotic Theory for Ignition and Extinction in Droplet Burning.* Combust. Flame 24 (1975) 89-98.

[6] Krishnamurthy, L, Williams, F. A., and Seshadri, K.: *Asymptotic Theory of Diffusion-Flame Extinction in the Stagnation-Point Boundary Layer.* Combust. Flame 26 (1976), 363-377.

[7] Chung, S.H. and Law, C.K.: *Structure and Extinction of Convective Diffusion Flames with General Lewis Numbers.* Combust. Flame 52 (1983), 59-79.

[8] Sohrab, S.H. and Williams, F.A.: *Extinction of Diffusion Flames Adjacent to Flat Surfaces of Burning Polymers.* J. Polymer Sci. 19 (1981) 2955-2976.

[9] Foutch, D.W. and T'ien, J.S.: *Extinction of a Stagnation-Point Diffusion Flame at Reduced Gravity.* AIAA J. 25 (1987) 972-976.

[10] Birkan, M. and Law, C.K.: *Asymptotic Structure and Extinction of Diffusion Flames with Chain Mechanism.* Combust. Flame 73, (1988)127-146.

[11] Du, J. and Axelbaum, R.L.: *The Effects of Flame Structure on Extinction of CH4/N2/O2 Diffusion Flames.* Proc. Combust. Inst. 26 (1996) 1137-1142.

[12] Christiansen, E. W., Tse, S. D. and Law, C. K.: *A Computational Study of Oscillatory Extinction of Spherical Diffusion Flames.* Combust. Flame 134, (2003) 327-337.

[13] Chen, R and Axelbaum, R.L.: *Scalar dissipation rate at extinction and the effects of oxygen-enriched combustion.* Combust. Flame 142 (2005) 62-71.

[14] Bonne, U.: *Radiative extinguishment of diffusion flames at zero gravity.* Combust. Flame 16 (1971), 147-159.

[15] Soharab, S.H., Liñán, A, and Williams, F. A.: *Asymptotic Theory of Diffusion-Flame Extinction with Radiant Loss from the Flame Zone.* Combust. Sci. Tech. 27 (1982) 143-154.

[16] Sibulkin, M.: *Free Convection Diffusion Flames from Burning Solid Fuels.* Prog. Erengy Combust. Sci. 14 (1988) 195-212.

[17] T'ien, J.S.: *Diffusion Flame Extinction at Small Stretch Rates: the Mechanism of Radiative Loss.* Combust. Flame 65 (1986) 31-34.

[18] Chao, B.H., Law, C. K., and T'ien, J. S.: *Structure and Extinction of Diffusion Flames with Flame Radiation.* Twenty-Third Symposium

(International) on Combustion, The Combustion Institute (1991), 523-531.

[19] Chan, S.H., Yin, J.Q., and Shi, B.J.: *Structure and extinction of methane-air flamelet with radiation and detailed chemical kinetic mechanism.* Combust. Flame 112 (1998), 445-456.

[20] Chao, B.H. and Law, C.K.: *Asymptotic Theory of Flame Extinction with Surface Reaction.* Combust. Flame 92 (1993) 1-24.

[21] Liu, F., Smallwood, G. J. Gulder, O.L. and Ju, Y.: *Asymptotic analysis of radiative extinction in counterflow diffusion flames of nonunity Lewis numbers.* Combust. Flame 121 (2000) 275-287.

[22] Maruta, K., Yoshida, M., Guo, H., Ju, Y. and Niioka, T.: *Extinction of low-stretched diffusion flame in microgravity.* Combust. Flame 112 (1998), 181-187.

[23] Mills, K. and Matalon, M.: *Extinction of Spherical Diffusion Flames in the Presence of Radiant Loss.* Proc. Combust. Inst. 27 (1998) 2535-2541.

[24] Patnaik, G. and Kailasanath, K.: *Numerical simulations of burner-stabilized hydrogen-air flames in microgravity.* Combust. Flame 99 (1994), 247-253.

[25] Atreya, A. and Agrawal, S.: *Effect of radiative heat loss on diffusion fames in quiescent microgravity atmosphere.* Combust. Flame 115 (1998), 372-382.

[26] Zhang, B. L., Card, J. M. and Williams, F. A.: *Application of rate-ratio asymptotics to the prediction of extinction for methanol droplet combustion.* Combustion and Flame 105 (1996), 267-290.

[27] Nayagam, B., Haggard, J.B., Colantonio, R.O., Marchese, A.J., Dryer, F.L., Zhang, B.L., and Williams, F.A.: *N-Heptane Droplet Combustion in Oxygen Helium Mixtures at Atmospheric Pressure.* AIAA J. 36 (8) (1998) 1369-1378.

[28] Dietrich, D.L., Haggard, J.B., Dryer, F.L., Nayagam, V., Shaw, B.D., and Williams, F.A.: *Droplet combustion experiments in spacelab.* Twenty-Sixth Symposium (International) on Combustion, The Combustion Institute. 26 (1996) 1201-1207.

[29] Tse, S.D., Zhu, D., Sung, C.J., Ju, Y. and Law, C.K.: *Microgravity burner-generated spherical diffusion flames: experiment and computation.* Combust. Flame 125 (2001), 1265-1278.

[30] Santa, K.J., Chao, B.H., Sunderland, P.B., Urban, D.L., Stocker, D.P., and Axelbaum, R.L.: *Radiative Extinction of Gaseous Spherical Diffusion Flames in Microgravity.* Combust. Flame, accepted pending revision (2007).

[31] Yoo, S.W., Christiansen, E.W., and Law, C.K.: *Oscillatory extinction of spherical diffusion flames: Micro-buoyancy experiment and computation.* Proc. Combust. Inst. 29 (2002) 29-36.

[32] http://mcrogravity.grc.nasa.gov/combusiton/index.htm

[33] Freidman, R. and Urban, D.L.: *Progress in fire detection and suppression technology for future space missions.* AIAA Space 2000 Conference and Exhibition, Long Beach, CA, Sept. 19-21, 2000.

[34] Liu, S., Chao, B.H. and Axelbaum, R.L.: *A Theoretical Study on Soot Inception in Spherical Burner-Stabilized Diffusion Flames.* Combust. Fame 140 (2005) 1-23.

[35] Sunderland, P.B., Axelbaum, R.L., Urban, D.L., Chao, B.H., and Liu, S.: *Effects of Structure and Hydrodynamics on the Sooting Behavior of Spherical Microgravity Diffusion Flames.* Combust. Flame 132 (2003) 25-33.

[36] Sunderland, P. B., Urban, D. L., Stocker, D. P., Chao, B. H. and Axelbaum, R. L.: *Sooting Limits of Microgravity Spherical Diffusion Flames in Oxygen-Enriched Air and Diluted Fuel.* Combust, Sci. Tech. 176, 2143–2164 (2004).